NRL Memorandum Report 6402

Equilibrium of Solar Coronal Arcades

JOHN M. FINN* AND JAMES CHEN

Geophysical and Plasma Dynamics Branch
Plasma Physics Division

**Science Applications International Corporation*
McLean, VA 22102

**University of Maryland*
College Park, MD 20742

March 27, 1989

SECURITY CLASSIFICATION OF THIS PAGE

REPORT DOCUMENTATION PAGE

Form Approved
OMB No 0704-0188

1a REPORT SECURITY CLASSIFICATION UNCLASSIFIED	1b RESTRICTIVE MARKINGS
2a SECURITY CLASSIFICATION AUTHORITY	3 DISTRIBUTION/AVAILABILITY OF REPORT Approved for public release; distribution unlimited.
2b DECLASSIFICATION/DOWNGRADING SCHEDULE	
4 PERFORMING ORGANIZATION REPORT NUMBER(S) NRL Memorandum Report 6402	5 MONITORING ORGANIZATION REPORT NUMBER(S)
6a NAME OF PERFORMING ORGANIZATION Naval Research Laboratory	6b OFFICE SYMBOL (If applicable) Code 4780
6c ADDRESS (City, State, and ZIP Code) Washington, DC 20375-5000	7b ADDRESS (City, State, and ZIP Code)
8a NAME OF FUNDING/SPONSORING ORGANIZATION ONR	8b OFFICE SYMBOL (If applicable)
8c ADDRESS (City, State, and ZIP Code) Arlington, VA 22203	10 SOURCE OF FUNDING NUMBERS PROGRAM ELEMENT NO: 61153N; PROJECT NO: RR033-02-44; TASK NO; WORK UNIT ACCESSION NO

11 TITLE (Include Security Classification)
Equilibrium of Solar Coronal Arcades

12 PERSONAL AUTHOR(S)
Finn,* J.M. and Chen, J.

13a TYPE OF REPORT	13b TIME COVERED	14 DATE OF REPORT (Year, Month, Day)	15 PAGE COUNT
Interim	FROM _____ TO _____	1989 March 27	70

16 SUPPLEMENTARY NOTATION
*Science Applications International Corporation, McLean, VA 22102

17 COSATI CODES			18 SUBJECT TERMS (Continue on reverse if necessary and identify by block number)
FIELD	GROUP	SUB-GROUP	MHD equilibria Solar corona Bifurcations

19 ABSTRACT (Continue on reverse if necessary and identify by block number)

Properties of two-dimensional straight (symmetric in z) magnetic arcade equilibria in the solar corona are studied within the framework of magnetohydrodynamics (~~MHD~~). Sequences of MHD equilibria are obtained by solving the Grad-Shafranov equation with the footpoint displacement and the entropy prescribed. It is shown that no multiple solutions, or bifurcations, result. This is to be contrasted with the approach of prescribing the axial magnetic field $B_z(\psi)$ or pressure $p(\psi)$, in which bifurcations do occur. The physical conditions for which the footpoint

(Continues)

20 DISTRIBUTION/AVAILABILITY OF ABSTRACT	21 ABSTRACT SECURITY CLASSIFICATION
☒ UNCLASSIFIED/UNLIMITED ☐ SAME AS RPT ☐ DTIC USERS	UNCLASSIFIED

22a NAME OF RESPONSIBLE INDIVIDUAL	22b TELEPHONE (Include Area Code)	22c OFFICE SYMBOL
J.D. Huba	(202) 767-3630	Code 4780

DD Form 1473, JUN 86 Previous editions are obsolete SECURITY CLASSIFICATION OF THIS PAGE

S/N 0102-LF-014-6603

19. ABSTRACTS (Continued)

displacement or entropy, as opposed to B_z or p, must be specified are discussed. It is argued that these conditions are more likely to occur in the corona than those conditions under which B_z and p may be prescribed. The lack of bifurcations indicates that equilibrium will not be lost as the footpoint displacement or entropy is increased. The limiting configurations for infinite footpoint displacement and infinite entropy are also discussed. It is shown that although the current density does become somewhat peaked, the total current in the peak region decreases as the system is sheared (or heated). In fact, the current in this peak region contains a rapidly decreasing fraction of the total current so that the limiting configuration is not one in which the current is concentrated into a current sheet.

CONTENTS

EQUILIBRIUM OF SOLAR CORONAL ARCADES

I. Introduction

Numerous fundamental issues remain unresolved concerning important energetic phenomena in the solar corona. For example, the possible mechanisms of solar flares, coronal mass ejections and various eruptive processes are not well understood. In these energetic events, energy release is manifested in the form of heating, radiation and/or mass motion in the coronal plasma. In addition, the corona evidently undergoes continual and pervasive (but perhaps less explosive) heating. Various theories have been proposed to explain these observed phenomena (for an overview, see, for example, Sturrock 1980). A substantial number of them assume that magnetic fields are the ultimate source of energy. This underlying assumption is strengthened by the recent observations (e.g., the Skylab mission, 1973) showing that the corona is a highly complicated system with magnetic fields and currents presumed to control the structuring and dynamics of coronal plasmas. As a result, it is important to understand the equilibrium and dynamical properties of magnetic structures in the corona.

In studying coronal magnetic fields, two dimensional magnetohydrodynamic (MHD) equilibrium models have received considerable theoretical attention. Such models are important both because of their relative simplicity and because many fundamental issues that arise in 2D may also exist in three dimensional systems. For example, linear arcades may be relevant to magnetic structures associated with neutral lines, where the normal component of the magnetic field $\underline{B}$ is zero. Such structures have been inferred from observations. An arcade may have a considerable amount of magnetic shear but typically varies weakly in the direction along the neutral line. As another example, cylindrically symmetric geometry has been used to model sunspot fields (Barnes and Sturrock 1972; Yang, Sturrock, and Antiochos 1986).

One frequently invoked scenario in which the magnetic energy of a structure in the corona is thought to be built up and stored is the following; as coronal magnetic field lines anchored in the photosphere are sheared, the structure evolves through a sequence of quasi-equilibrium configurations, stressing the field lines and building up magnetic energy. As the twist of field lines in the corona is increased, equilibrium limits may be exceeded, resulting in catastrophic loss of equilibrium and sudden

Manuscript approved January 26, 1989.

release of magnetic energy. This scenario is an appealing one because of the ubiquity of coronal magnetic fields. A similar scenario in which loss of equilibrium occurs as a result of increasing the pressure, a measure of the internal energy of the plasma, has also been suggested. The issues addressed in this paper pertain to sequences of equilibria and loss of equilibrium. We believe that these issues are relevant in both two- and three-dimensional structures.

In this paper we specialize to straight arcade equilibria such that $\partial/\partial z = 0$ for all variables. Figure 1 shows a schematic drawing of a linear arcade field line configuration. Such arcades have been studied in the context of quasistatic evolution of equilibria (Barnes and Sturrock 1972; Low 1977,1982; Jockers 1978; Birn, Goldstein, and Schindler 1978; Heyvaerts et al. 1982; Yang, Sturrock, and Antiochos 1986; Zwingmann 1987; Priest 1988; Klimchuk, Sturrock, and Yang 1988) as well as dynamical evolution (Wu, Bao, and Tandberg-Hanssen 1987; Mikic, Barnes, and Schnack 1988.) Figure 1 shows schematically the coordinate system and a representative field line. The field lines are labelled by the flux $\psi = A_z(x,y)$. The footpoints are displaced in z by an amount $d(\psi)$ in the photosphere S. We adopt the usual ideal MHD line-tying condition in the photosphere. Then, the footpoint displacement can be specified by plasma motion in the photosphere. Arcade equilibrium studies have been previously performed with the idea that magnetic energy $W = \int dV B^2/8\pi$ increases as the shear is increased and that because of this increase, MHD instability or loss of equilibrium is possible. A standard method for obtaining equilibrium solutions is to solve the Grad-Shafranov equation. The most natural approach to solving this equation for a linear arcade is to specify the axial component of the magnetic field $B_z(\psi)$ and/or the pressure $p(\psi)$. [In the following, when we write $p = p(\psi)$, we assume that the relevant length scales in the corona are smaller than the gravitational scale height in the corona.] Thus, in many of the earlier papers, loss of equilibrium, or bifurcation, has been studied in the context of arcade equilibria with B_z specified (for an overview, see, for example, Birn and Schindler 1981). Another approach is to treat the equilibrium problem as a time dependent one involving Clebsch variables and introduce artificial viscosity or drag (Chodura and Schluter 1981; Yang, Sturrock and Antiochos 1986; Klimchuck, Sturrock and Yang 1988). This

"magneto-frictional" method allows the system to find a stable equilibrium for specified footpoint displacement.

By solving the Grad-Shafranov equation with prescribed axial field B_z, bifurcations have been found in the two-dimensional force-free limit (Jockers 1978). Having found multiple solutions, Jockers then pointed out that it may be more physically significant to specify the footpoint displacement rather than B_z and that bifurcations may not exist with respect to specification of footpoint displacement $d(\psi)$. The reason is that, in the idealized limit of perfectly conducting photosphere and corona, the specified footpoint displacement can be conserved as the system adjusts to find its equilibrium, while the coronal plasma posseses no physical mechanism which can hold B_z (or equivalently the transverse current perpendicular to z) fixed during this process. It also depends upon the assumption that inertia dominates magnetic forces in the photosphere ($\rho v^2/2 \gg B^2/8\pi$) and therefore the actual fields obtained in the arcade equilibrium do not influence the footpoint motion. In a recent comprehensive and detailed study, Zwingmann (1987) obtained sequences of arcade equilibria by varying footpoint displacement and pressure. The conclusion of this work is that no multiple solutions (i.e., bifurcations) exist if footpoint displacement is prescribed, confirming the suggestion of Jockers (1978), but that multiple solutions do exist if pressure $p(\psi)$ is prescribed. Thus, it was argued that the onset conditions for solar eruptive processes might be determined by bifucations with respect to increasing the pressure. In this work, Zwingmann used an iteration method developed by Keller (1977). Priest (1988) has also suggested that if the pressure is increased beyond a certain critical point, eruptive motion (e.g., coronal mass ejections) may result due to loss of equilibrium. Recently, Klimchuck, Sturrock and Yang (1988) also found that the magnetic energy of a linear dipole field increased indefinitely with increasing footpoint shear.

Clearly, it is important to distinguish between specifying $B_z(\psi)$ and specifying footpoint displacement $d(\psi)$ because the bifurcation properties are completely different. An analogous distinction exists between specifying the pressure $p(\psi)$ and specifying the entropy $s(\psi)$, both quantities being measures of internal energy of the plasma. The entropy can be defined in terms of the heat contained between flux surfaces (Sec. II).

In the limit of adiabatic coronal plasma, the entropy is a conserved quantity. In the corona, we expect perpendicular thermal conduction to be smaller than parallel conductivity and different flux surfaces are effectively thermally isolated. If, in addition, the parallel heat flux between the corona and the photosphere is small enough, then the corona is thermally isolated along the field lines from the photosphere. If these conditions are satisfied, then the adiabatic limit may be approximately valid and the entropy $s(\psi)$, like the footpoint displacement, is conserved as the system adjusts to find its equilibrium. Here, it is implicitly assumed that the Alfven speed or magnetosonic speed is sufficiently fast that radiation and thermal conduction to the photosphere are negligible on the time scale of relaxation to equilibrium. We also discuss in Sec. II an alternative limit of an isothermal model, corresponding to clamping of temperature by radiative processes or by parallel thermal conduction. This limit has essentially the same mathematical form as the adiabatic limit, but with adiabatic index of unity. In contrast, it appears that there is no such limiting case, arising from a reasonable energy equation for the coronal plasma, in which the pressure $p(\psi)$ is conserved as the flux surfaces adjust themselves to find an equilibrium.

In the present paper, we present a method to solve the Grad-Shafranov equation for linear arcades with prescribed footpoint displacement $d(\psi)$ or entropy $s(\psi)$. Using this technique, we consider the bifurcation properties of equilibrium arcades. We find that no multiple solutions exist if $d(\psi)$ is increased, in agreement with Zwingmann (1987). However, we find that there are no multiple solutions if the entropy $s(\psi)$, rather than the pressure, is specified. In situations where the entropy rather than the pressure is to be specified, the bifurcations with respect to the pressure are of mathematical rather than physical significance.

We also consider questions regarding the formation of sheet current in "open field configurations" which have been postulated as the limit of infinite footpoint displacement (Barnes and Sturrock 1972; Yang, Sturrock, and Antiochos 1986; Aly 1984, 1985). This configuration is a potential field ($\mathbf{j} = 0$) except along the current sheet. The development of sheet currents ("tangential discontinuities" of the magnetic field) has been an active area of investigation since it was suggested by Parker (1972, 1983) as a possible source of coronal heating. See also van Ballegooijen (1985),

Zweibel and Li (1987), Low and Wolfson (1988) and Antiochos (1988). We find that as $d(\psi)$ is increased, the current density j_z does become more peaked but that the maximum value of j_z increases only slowly, if at all, with footpoint displacement, and that, relative to the total current I_z, a decreasing fraction of current is carried by the current peak. We conclude that the field does not approach the postulated open field configuration. By the same token, if the entropy $s(\psi)$ is increased, the current density j_z becomes increasingly peaked but a decreasing fraction of current is carried by the peak relative to the total current I_z.

In Sec. II we formulate the MHD equilibrium problem for a straight arcade with pressure and gravity. We discuss the specification of footpoint displacement and entropy and relate the former to the familiar Clebsch representation for fields. In Sec. III, we discuss the computational method used to obtain the equilibria when footpoint displacement or entropy is prescribed. We then show results obtained by this method for various profiles of photospheric flux, footpoint displacement, and entropy. We compare these results with some simple analytic cases and show estimates based upon scaling for large footpoint displacement or entropy. The relevance to the formation of a sheet current as $d \to \infty$ or $s \to \infty$ is discussed. Sec. IV contains discussions of the results and their significance to coronal observations. The salient results are summarized in Sec. V.

II. Linear Arcade Equilibria

a) Basic Equations

The geometry considered in this paper is that of a linear arcade with a straight neutral line. We choose coordinates as shown in Fig. 1, with $\hat{e}_y$ the unit vector normal to the surface S(y = 0) corresponding to the photosphere and x labelling the non-ignorable direction in S. We adopt the usual assumption that the corona has infinite electrical conductivity (on the time scales of interest) and that the photosphere is infinitely conducting and massive. Then, the field line footpoints are line-tied in the surface S. In such a geometry where z is the ignorable direction, the magnetic field can be represented by

$$\mathbf{B} = \nabla\psi \times \hat{e}_z + B_z\hat{e}_z \ , \tag{1a}$$

where the flux function $\psi(x,y)$ is the z-component of the vector potential. The current density $\mathbf{j} = \nabla \times \mathbf{B}$ (in normalized units $c/4\pi = 1$) is then given by

$$\mathbf{j} = \nabla B_z \times \hat{e}_z - \nabla^2\psi\hat{e}_z \ . \tag{1b}$$

Including the effects of pressure p and gravity, the equation of motion is

$$\mathbf{j} \times \mathbf{B} - \nabla p - mgn\hat{e}_y = 0, \tag{2}$$

where n is the ion (or electron) density and m is the ion mass. The component of eq. (2) in the z-direction gives $\mathbf{B}\cdot\nabla B_z = 0$ which implies

$$B_z = B_z(\psi). \tag{3}$$

The quantity $B_z(\psi)$ can be related in a simple manner to the transverse current per unit length in the z direction. Consider a closed path around a rectangle defined by $\psi_1 < \psi < \psi_2$, $0 < z < L$ on the photospheric surface (S). Ampere's law $\oint \underline{B} \cdot d\underline{l} = I$ then yields $[B_z(\psi_1) - B_z(\psi_2)]$ as the transverse current per unit length in z flowing between the flux surfaces $\psi = \psi_1$ and $\psi = \psi_2$. Writing the pressure, temperature and density as functions of the nonorthogonal coordinates ψ and y, we find that the component of eq. (2) parallel to $\underline{B}$ leads to

$$\frac{\partial}{\partial y} p(\psi,y) = - \frac{mgp(\psi,y)}{2kT(\psi,y)} \tag{4a}$$

where k is Boltzmann constant, T is the electron temperature and m is the ion mass. This equation can be solved to give

$$p(\psi,y) = p(\psi,0)\exp\left(- \frac{mg}{2k}\int_0^y \frac{dy'}{T(\psi,y')}\right) . \tag{4b}$$

For the special case $T = T(\psi)$, we find

$$n(\psi,y) = n_o(\psi)\exp[- mgy/2kT(\psi)]. \tag{4c}$$

Here, $p(\psi,0)$, $n(\psi,0)$ are the pressure and density on S. Equation (4a) simply states that the plasma is in hydrostatic equilibrium along the field lines. Substituting eqs. (3) and (4b) in the $\nabla\psi$ component of eq. (2) leads to the Grad-Shafrarov (G-S) equation

$$\nabla^2\psi = - \lambda(\psi)B_z(\psi) - \frac{\partial p}{\partial \psi} , \tag{5a}$$

where

$$\lambda(\psi) \equiv \frac{dB_z}{d\psi} ,$$

and

$$p(\psi,y) = 2n(\psi,y)kT(\psi,y). \qquad (5b)$$

In the remainder of this work, we adopt the assumption that y is much smaller than the gravitational scale height in the corona $h = 2kT/mg$ so that force balance along the field lines is achieved by having pressure constant along the field lines in the corona, giving $p = p(\psi)$. We will also assume that paralle thermal conduction dominates in the corona (but not in the transition zone, chromosphere, or the photosphere) so that $T = T(\psi)$. It follows from eq. (5b) that density is also constant along field lines, $n = n_o(\psi)$. An important special case occurs if the plasma beta $\beta = 2p/B^2$ is small, giving the force free condition $p = 0$.

The boundary conditions which we specify on eq. (5) are that the flux $\psi(x,0)$ is given on the surface S and is assumed to be constant (zero, without loss of generality) for $(x,y) \to \infty$. This, of course, determines the component $B_y = -\partial\psi(x,0)/\partial x$ normal to S. In practice, these conditions are replaced by those specifying $\psi(x,0)$ for a finite interval $0 < x < a$ on S and by requiring ψ to be zero on the surfaces $x = 0$, $x = a$ and $y = L$. See Figure 2. We will return to the implications of these boundary conditions on a box of finite size (in x,y) in Sec. III. Mathematically, the G-S equation (5) is usually posed as a nonlinear boundary value problem by specifying the nonlinear functions $B_z(\psi)$ and $p(\psi)$. This specification can lead to multiple solutions (bifurcations). However, it was suggested by Jockers (1978) that B_z is not a physically specifiable quantity in the corona and that bifurcations may not exist if the footpoint displacement is specified. This point was recently demonstrated by Zwingmann (1987), who also found bifurcations with respect to specifying the pressure $p(\psi)$.

b) Specifiability of Physical Quantities

In this section, we discuss the specifiability of a number of physical quantities. For this purpose, it is helpful to use an imaginary two-step process. Consider a system in equilibrium (e.g., $\mathbf{j} \times \mathbf{B} = 0$). Suppose a physical quantity (e.g., footpoint displacement) is changed holding all other quantities fixed (first step). Then the system is no longer in equilibrium and it must relax to a new equilibrium (second step). If the

physical quantity in question is a conserved quantity during the relaxation process, then it retains the given value after reaching the new equilibrium. Such a conserved quantity can be specified. If, on the other hand, the quantity is not a conserved quantity, then it also changes during the relaxation process so that it cannot be held fixed. In this case, a specified value need not be attainable.

For example, if the footpoint displacement is increased from that of an initial equilibrium, then it is a constant of the motion in the subsequent relaxation motion of the plasma in the limit where the photosphere is assumed to be infinitely conducting and infinitely massive. It is mathematically allowable to compute equilibria by specifying $B_z(\psi)$. However, if B_z is increased from that of an equilibrium, the coronal plasma cannot hold it fixed during relaxation to a new equilibrium. It is not a constant of the motion under ideal MHD motion. That is, a specified value of B_z need not be attainable from the initial equilibrium. If one is to study quasi-static response to a slow photospheric motion, slow enough so that the coronal inertia is negligible, then the footpoint displacement, rather than B_z, must be specified.

The internal energy of a volume of plasma can be represented by the pressure p or entropy s (to be defined below). If the entropy of an initial equilibrium is increased, then it is conserved in the relaxation process in the limit where the plasma is assumed to be adiabatic on the relaxation time scale. That is, there exists a limit in which the plasma can be described by an equation conserving the entropy (eq. [6d]). However, no conservation law based on a reasonable energy equation has been identified in which the pressure is conserved and which is suitable for the coronal environment. A third limit which may be relevant to the corona is the isothermal limit.

In reality, coronal plasmas need not correspond strictly to any of the limiting cases, in which case none of the physical quantities discussed would be specifiable rigorously. Specification of a quantity is physically meaningful only in a suitable limit in which the quantity is a conserved constant of the motion. Nevertheless, it may still be useful to adopt one or more of the limiting assumptions and explore theoretical issues. In the next section, we discuss the limiting conditions under

which the above quantities are conserved. Additional physical implications of specifiability are discussed in Sec. IV.

c) Footpoint Displacement and Entropy

By integrating the z-component of the field line equations $d\underline{x}/ds = \underline{B}/B$ (ds measures arc length along the magnetic field) from footpoint 1 to footpoint 2, we find

$$d(\psi) = B_z(\psi)V'(\psi), \tag{6a}$$

where

$$V'(\psi) \equiv \int_1^2 ds/B \tag{6b}$$

Here, $V(\psi) = \int dxdy = \int ds_p d\psi/|\nabla\psi| = \int ds d\psi/B$, where ds_p measures arc length in the transverse plane. The quantity $V(\psi)$ is proportional to the area in the x-y plane enclosed by the flux surface labelled by ψ and $V'(\psi) = dV/d\psi$, so that $V'(\psi)d\psi$ is the volume per unit length in the z direction between the flux surfaces labelled ψ and $\psi + d\psi$. Also, if we define $\Phi(\psi) = \int dxdyB_z$ to be the axial flux bounded by the flux surface labelled by ψ and the photosphere, then we find from eq. (6a)

$$d(\psi) = \frac{d\Phi}{d\psi} .$$

During the process of increasing $d(\psi)$ with respect to time, the velocity v_z produces a tangential electric field $E_x = v_z B_y$ on S, which is responsible for the change of Φ in time. Thus, the footpoint displacement is directly specifiable through the boundary conditions and is a constant of motion in any process in which the plasma relaxes to equilibrium on a time scale faster than the time scale for the change in footpoint displacement. We point out that Clebsch variables have also been used in specifying footpoint displacement (e.g., Yang, Sturrock, and Antiochos 1986; Klimchuck, Sturrock, and Yang 1988). See Appendix A.

If we assume that the coronal gas is an ideal gas, then the entropy $\sigma'(\psi)d\psi \equiv (d\sigma/d\psi)d\psi$ of this volume is such that

$$\sigma'(\psi) = Q\ln(pV'^{\gamma})$$

where the contribution $\gamma Q\ln(d\psi)$ has been dropped because only the difference in entropy is significant. Here, $\gamma = 5/3$ is the adiabatic index. For convenience, we will refer to the following quantity $s(\psi)$ as "entropy" in this paper but the above relationship is understood;

$$s(\psi) = p(\psi)[V'(\psi)]^{\gamma} . \tag{6c}$$

Then $s(\psi) = \exp[\sigma'(\psi)/Q]$.

In our formulation, the entropy $s(\psi)$ replaces the pressure $p(\psi)$ as the specified quantity. It can be shown that the entropy is conserved in MHD directly without resorting to thermodynamic considerations. Specifically, the entropy is conserved by adiabatic motions satisfying the adiabatic law

$$\frac{\partial p}{\partial t} + \underset{\sim}{v}\cdot\nabla p + \gamma p\nabla\cdot\underset{\sim}{v} = 0. \tag{6d}$$

This is easily seen by noting that $p^{1/\gamma}$ satisfies the same continuity equation as the density $\partial n/\partial t + \nabla\cdot(n\underset{\sim}{v}) = 0$. Then, the quantity $S \equiv \int p^{1/\gamma}dV$ is conserved if there is no transport of plasma across the flux surfaces. This condition holds if the plasma satisfies ideal MHD so that the flux surfaces move the the fluid. Here, the integral is over the volume between any two flux surfaces. If we take a small volume δV between two closely spaced flux surfaces at ψ and $\psi + \delta\psi$, then δV is proportional to $V'(\psi)\delta\psi$. Therefore, S is equal to $p(\psi)^{1/\gamma}V'(\psi)\delta\psi$. Since $\delta\psi$ is conserved for ideal MHD motions, the entropy $s(\psi) \equiv S^{\gamma}/\delta\psi^{\gamma}$ is conserved for an adiabatic process. Grad, Hu, and Stevens (1975) have developed algorithms to specify

entropy in toroidal systems. In the arcade geometry treated here, an additional assumption of negligible heat flux to the photosphere is required. As in the justification for specifying footpoint displacement, the entropy is the directly specifiable response to varying the internal energy of the plasma in the adiabatic limit. Note that pressure is not conserved in adiabatic processes. In the following discussion, we will adopt the scenario in which the internal energy of the plasma is specified by specifying the entropy $s(\psi)$.

In the isothermal limit, the temperature remains fixed (perhaps by some radiative proces) during the relaxation to equilibrium. An isothermal plasma obeys a relationship similar to eq. (6c). If the mass $M(\psi)$ contained under each flux surface is conserved (no photospheric sources), then $M'(\psi) = mn(\psi)V'(\psi)$ may be specified, where

$$M(\psi) = m\int n(\psi)\frac{d\psi ds}{B} .$$

Mathematically, it is simple to see (Appendix B) by comparing eqs. (6a) and (6c) that $p(\psi)$ can be identified with $(1/2)B_z(\psi)^2$ and $s(\psi)$ with $(1/2)d(\psi)^2$, having $\gamma = 2$ and $\gamma = 5/3$, respectively, a rather insignificant difference. For the isothermal case, $s(\psi)$ is replaced by $M'(\psi)$ with $\gamma = 1$.

d) Simple Analytic Equilibria

We now illustrate some basic physical features of equilibrium solutions of eq. (5) using force-free examples. A particularly simple example can be given by the form $B_z(\psi) = \lambda_o\psi$ where λ_o is a constant. Then, the G-S equation (eq. [5a]) reduces to the Helmholtz equation

$$\nabla^2\psi + \lambda_o^2\psi = 0. \qquad (7)$$

Solutions confined to $0 < x < a$ with $\psi(0,y) = \psi(a,y) = 0$ but extending to $y = \infty$ $(0 < y < \infty)$ have the form

$$\psi = \psi_o \sin\left(\frac{n\pi x}{a}\right) e^{-k_n y}, \tag{8}$$

with $k_n = [(n\pi/a)^2 - \lambda_o^2]^{1/2}$. This equilibrium is the two-dimensional, linear arcade analogue of the Lundquist (1951) solution (one-dimensional, cylindrical geometry) and has been used by Heyvaerts and Priest (1984) in a model for coronal heating. If the flux on the surface S is taken to be $\psi(x,0) = \sin(\pi x/a)$, then only n = 1 occurs. In this case, the imposed λ_o must satisfy $k_1^2 > 0$ or $\lambda_o < \lambda_c \equiv \pi/a$. That is, if it were physically reasonable to specify λ_o [$B_z(\psi) = \lambda_o \psi$], then one might expect to encounter a violent loss of equilibrium as λ_o is increased past $\lambda_c = \pi/a$.

Using eq. (6a), we obtain

$$d(\psi) = B_z(\psi) \int_{x_1}^{x_2} \frac{dx}{B_x} \tag{9a}$$

$$= -\frac{2\lambda_o}{k_1}(x - x_o), \tag{9b}$$

where $x_o = a/2$ is the point where ψ is maximum ($\psi = \psi_o$) on S with $B_y = 0$, and $x = x(\psi)$ is the inverse of $\psi = \psi(x,0)$. Also, x_1 and x_2 are the x values where the flux surface labelled by ψ crosses the photosphere. The footpoint displacement d is linear in x and the maximum in magnitude of d occurs at x = 0, x = a and equals

$$d_{max} = \frac{\lambda_o a}{\left[(\pi/a)^2 - \lambda_o^2\right]^{1/2}} \tag{10a}$$

Since the <u>form</u> of $d(\psi)$ is unchanged by λ_o, we can consider d_{max} to be specified and λ_o to be computed after the fact:

$$\lambda_o = \left(\frac{d_{max}}{a}\right) \frac{\pi}{\left(a^2 + d_{max}^2\right)^{1/2}} . \tag{10b}$$

Since the maximum of B_z, $(B_z)_{max}$, equals $\lambda_o\psi_o$, we can consider eq. (9) to be a computation of $d(\psi)$ when $B_z(\psi)$ is specified and eq. (10b) to be a computation of $B_z(\psi)$ when $d(\psi)$ is specified. In the latter case, no equilibrium catastrophe is reached; as $d_{max} \to \infty$, λ_o merely increases, approaching the limiting value $\lambda_c = \pi/a$. This model is illustrative, especially since it also shows the relationship between $d_{max} \to \infty$ and vertical flux surface expansion, which is equivalent to $k_1 \to 0$ (see eq. [8]). However, it has two special properties that do not hold in general; (i) λ_o, or equivalently $(B_z)_{max}$, monotonically increases with d_{max} and (ii) the form of $B_z(\psi)$ does not change as d_{max} changes with the form of $d(\psi)$ fixed.

III. Linear Arcade Equilibria

a) Some General Properties

In this section, some general properties of force-free configurations are discussed. First, we point out that an arcade equilibrium on the half space $-\infty < x < \infty$, $y > 0$ with flux ψ and footpoint displacement $d(\psi)$ specified on the x-axis, must have a surrounding region of potential field with $\lambda(\psi) = dB_z/d\psi = 0$ or at least with B_z and $dB_z/d\psi$ approaching zero sufficiently fast as $(x, y) \to \infty$. The footpoint displacement in the our model is such that $d \to 0$ as $x \to \pm\infty$, representing an arcade whose footpoint shear is confined to a finite extent in x in the photosphere. For this type of arcades, $\lambda(\psi)$ cannot be constant everywhere or asymptotically approach a non-zero constant. This can be seen by the following consideration. Here, we specialize to the case in which $\psi(x,0)$ is an even function about $x = 0$, monotonically decreasing for $x > 0$. Without loss of generality, we may demand that $\psi(x,0) \to 0$ as $x \to \pm\infty$. As a concrete example, assume $B_z(\psi) = \lambda_0\psi + B_0$, where B_0 is the B_z field at infinity. Suppose $\lambda_0 \neq 0$ so that $dB_z/d\psi \neq 0$ for all x. Now, suppose, for contradiction, that $B_0 \neq 0$. Then, $V'(\psi)$ becomes infinite for $\psi \to 0$ as $(x, y) \to \infty$. This implies (eq. [6a]) that, if $B_0 \neq 0$, then an infinite footpoint displacement $d(\psi)$ must result as $x \to \pm\infty$ and $\psi \to 0$. Therefore, the outermost flux surfaces must have $B_z = B_0 = 0$ at $x = \pm\infty$ if $d(\psi)$ is to vanish. Thus, we set $B_0 = 0$. Then, eq. (5a) leads to $\nabla^2\psi + \lambda_0^2\psi = 0$. If $\phi(k)$ is the Fourier transform of $\psi(x,0)$, the solution takes the form

$$\psi(x,y) = \int_{-\infty}^{\infty} dk\,\phi(k)\cos(kx)e^{-\mu(k)y} \qquad (11)$$

where $\mu(k) = (k^2 - \lambda_0^2)^{1/2}$. Note that

$$\int_{-\infty}^{\infty} dx\,\psi(x,0)\cos(kx) = 2\pi\phi(k).$$

Since $\psi(x,0)\cos(kx)$ is even in x, $\phi(k)$ is nonzero in general. In particular, $\phi(k)$ is nonzero for $k < \lambda_0$. The solution must then be oscillatory. This physically unacceptable behavior occurs because of the

supposition $\lambda_0 \neq 0$. For a more general case with arbitrary $B_z(\psi)$, the above argument shows that $\lambda(\psi) = dB_z/d\psi$ must approach zero as $\psi \to 0$. If, say $\lambda(\psi)$ is assumed to be a constant $\lambda_0 \neq 0$ in some region $y > y_c$, then the above argument applies to the region $-\infty < x < \infty$, $y > y_c$, again with the result that ψ cannot be well behaved for $y \to \infty$. This is a generalization to the half-space with line-tying of the well known virial theorem that a plasma cannot be confined by its own fields. As another example of virial theorem application, we note that if there is no potential field surrounding the localized $j \neq 0$ region, then the structure cannot be force-free and the pressure must be lower in that region than in the surrounding region. This has been shown for a three-dimensional "toroidal" solar current loop structure (Xue and Chen 1983). Note that an earlier example of a force-free field without a surrounding potential field (Low 1977) is a configuration in which the footpoint displacement has an infinite extent in the photosphere and asymptotically approaches a finite maximum at $x = \pm\infty$.

b) Effects of Finite Computational Domains

As mentioned earlier, the boundary conditions are that $\psi(x,0)$ is specified for $0 < x < a$ on S, and $\psi = 0$ on the remaining three surfaces; the two side walls at $x = 0$, $x = a$, and the top wall at $y = b$. The flux $\psi(x,0)$ is chosen to be even about $x = a/2$ so that the maximum value ψ_0 occurs at $x = a/2$ and ψ decreases monotonically to zero at $x = 0$ and $x = a$. We consider a current-carrying plasma confined away from the side and top walls. Let the outermost flux surface of the current-carrying region be $\psi = \psi_v$. This surface intersects the surface S at $x = x_v$ and $x = a-x_v$ where $x_v = x(\psi_v)$. The flux surfaces outside this region ($\psi < \psi_v$) are then potential flux surfaces. Based on the arguments of the preceding section, we specify $d(\psi)$ to be zero (thus $B_z = 0$) on the potential flux surfaces. For $\psi_v \simeq 0$, the current fills the entire box. Then a force-free configuration is supported by the walls and the form of $B_z(\psi)$ for specified $d(\psi)$ will be seriously modified. For larger ψ_v, a force-free structure is supported by the surrounding potential flux, which in turn is supported by the walls. If ψ_v is sufficiently large, then the interface surface $\psi = \psi_v$ is sufficiently far from the walls and its shape is determined by the

actual force balance requirement. In this section, we will discuss the generic effects of the finiteness of the computational domain on the solution. Hereafter, we use dimensionless variables with x,y, $d(\psi)$ scaled to a ($0 < x < 1$). The flux function ψ is scaled to its maximum ψ_o, B_z is scaled to ψ_o/a, and p is scaled to ψ_o^2/a^2.

We expect the general form of $d(\psi)$ to be linear in x near the neutral line at $x = a/2$ [as it is in eq. (9b)] and vanish as the potential region is approached. Clearly, $d(\psi)$ must vanish at $x = a/2$ because the field line has zero length there. Furthermore, if the magnetic field is regular in that vicinity, then d is linear in x unless B_z is finite and <u>both</u> components B_x and B_y vanish at $x = a/2$, $y = 0$. Otherwise, an O-point rises above the boundary surface S. This is inconsistent with specifying $d(\psi)$; if an O-point forms, then d must have a step function discontinuity.

As a first example, we have computed force-free equilibria with d(x) of the form

$$d(x) = d_o\left(x - \frac{a}{2}\right)\tanh\left[\frac{(x - x_v)}{W(a/2 - x_v)}\right] \qquad \begin{matrix} x_v < x < a/2 \\ (\psi > \psi_v), \end{matrix} \tag{12a}$$

$$= 0 \qquad \begin{matrix} x < x_v \\ (\psi < \psi_v) \end{matrix} \tag{12b}$$

and anti-symmetric about $x = a/2$. The G-S equation is solved iteratively for specified $d(\psi)$. The computational method is described in Appendix B. In Figure 2a, we show the flux surfaces for a representative equilibrium. We have used $\psi(x,0) = \psi_o \sin(\pi x/a)$ with $\psi_o = 1$, the height of the integration box $b/a = 2$, and $\psi_v = 0.195$, for which $x_v = 0.0625$. The maximum footpoint displacement is specified to be $d_{max} = 1.85$ and we have chosen $W = 0.1$. The coefficient d_o is adjusted so that the specified value of d_{max} is obtained. The short-dashed contour corresponds to $\psi = \psi_v$ where $j_z = 0$ and $d = 0$. All the current is contained inside ($\psi > \psi_v$) the $\psi = \psi_v$ surface. Thus, the outer boundary surface of the $j \neq 0$ region is removed from the computational box by a moderate amount. The long-dashed contour corresponds to the flux surface $\psi = \psi_w$, defined to be the flux surface such that $d(\psi_w) = d_{max}/2$. (For this example, we have $d(\psi_w) = 0.92$, $x_w = 0.08$, and $\psi_w = 0.25$.) The bulk of the current is actually enclosed by this surface, farther away from the walls than the ψ_v surface. Figure 2(b)

shows the footpoint displacement profile. (This figure shows d only for 0 < x < 0.5. The overall sign is reversed from that of eq. [12a] for convenience.) The above form has the general feature that the anti-symmetric footpoint displacement is zero for $0 < x < x_v$ with most of the footpoint displacement shear concentrated in $x_v < x < x_m$ where $x_m \simeq x_v + W(a/2 - x_v)$ is where the maximum footpoint displacement $d_{max} = d(x_m)$ occurs. In $x_m \lesssim x \lesssim (a - x_m)$, d(x) is essentially linear so that field lines on different flux surfaces are parallel and unsheared. For larger values of W, the footpoint displacement shear is less concentrated.

In Fig. 2(c), we have plotted $B_z(\psi)$ versus ψ for $0 < \psi < 1$. (Recall that on the surface S, $\psi = 0$ for $x = 0$ and $x = 1$, and $\psi(x=0.5, y=0) = \psi_o = 1$.) We see that $B_z(\psi)$ is linear in ψ near ψ_o and deviates from linearity in the region of maximum shear in the footpoint displacement. In Fig. 2(d), we show $\lambda(\psi) = dB_z/d\psi$ as a function of ψ. As expected, $\lambda(\psi)$ has its maximum variation in the region of maximum shear in $d(\psi)$.

In Fig. 3, the quantity $(B_z)_{max} \equiv B_z(x=0.5,y=0)$ is plotted as a function of d_{max} for a number of model equilibria. Curve 1 is a plot of eq. (10b), a linear force-free configuration confined horizontally to $0 \lesssim x \lesssim 1$ but extending vertically to $y = \infty$. For this system, $(B_z)_{max}$ (thus λ_o) is linear in d_{max} for small d_{max} and asymptotically approaches π/a as $d_{max} \to \infty$. For small d_{max}, $V'(\psi)$ is, to lowest order, the value for the potential field ($d_{max} = 0$) and $(B_z)_{max}$ is proportional to d_{max} (see eq. [6a]). For $d_{max} \to \infty$, on the other hand, the increase in d_{max} causes an expansion of flux surfaces, i.e. an increase in $V'(\psi)$, with $(B_z)_{max}$ approaching a constant. Curve 2 of Fig. 3 is for the solution of eq. (7) for a finite height b, where the boundary condition is $\psi(x, y=b) = 0$. The equilibrium can be described analytically by

$$\psi(x,y) = \sin\left(\frac{\pi x}{a}\right)\sinh k_1(b-y)/\sinh k_1 b, \qquad (13)$$

where $k_1 = [(\pi/a)^2 - \lambda_o^2]^{1/2}$ for $\pi/a > \lambda_o$. For $\lambda_o > \pi/a$, eq. (13) is replaced by

$$\psi(x,y) = \sin\left(\frac{\pi x}{a}\right)\sin k_1(b - y)/\sin k_1 b, \qquad (14)$$

where $k_1 = [\lambda_o^2 - (\pi/a)^2]^{1/2}$. For this equilibrium of finite height, the

functional form of $d(\psi)$ (not merely the amplitude d_{max}) changes with λ_o so that, unlike the infinite height equilibrium given by eq. (8) or eq. (10b) (curve 1), specifying λ_o or $(B_z)_{max}$ is not essentially equivalent to specifying d_{max}. For the infinite height case, eq. (9b), the profile of d remains linear in x and that of B_z linear in ψ for all values of λ_o, or equivalently, for all values of d_{max}. Nevertheless, the curves 1 and 2 are similar. Curve 2, however, shows that $(B_z)_{max}$ (or λ_o) can increase beyond the limit $\lambda_o \to \pi/a$, in contrast with curve 1. For curve 2, the finite height (b) of the box prevents the flux surfaces from expanding freely as $d_{max} \to \infty$. In this case, $V'(\psi)$ cannot increase without bounds and d_{max} can increase only through an increase in $(B_z)_{max}$ (see eq. [6a]). However, for this equilibrium, the flux function ψ takes the form of eq. (14) for $\lambda > \pi/4$ and an O-point appears at $x = a/2$ above the surface S ($y > 0$) if $k_1 b > \pi/2$, or $\lambda_o > (\pi/a)(1 + a^2/4b^2)^{1/2}$. For $b/a = 2$, the parameter used in curves 2 and 3, this gives $\lambda = 3.24$. We have not attempted to extend d_{max} past this point. Curve 3 is the equilibrium for a footpoint displacement profile given by eq. (12a) with $\psi_v = 0.195$ and $W = 0.1$, the equilibrium shown in Fig. 2a. This equilibrium is numerically computed in the same finite box as for curve 2. As in curve 2, $(B_z)_{max}$ increases past π/a as d_{max} increases, albeit slowly, because of the finite size of the computational domain. Presumably, $(B_z)_{max}$ continues to increase, at a faster rate with respect to d_{max}, as d_{max} increases further. However, the non-zero current region (inside the short-dashed flux surface in Fig. 2a) is detached from the side walls (and the region $\psi_v < \psi < \psi_w$ has less current than in Fig. 2a). Thus there is relatively more room to expand than in the configuration described by curve 2. This flexibility for the flux surfaces to expand against the potential flux surfaces is responsible for the smaller values of $(B_z)_{max}$ for large d_{max}. The difference in the slopes of curve 3 and curve 1 (or curve 2) is not physically significant, but is related to the fact that d_{max} itself has a different meaning for the two very different profiles of $d(\psi)$, given by eq. (9b) and eq. (12). Curve 3 shows that the numerically computed equilibrium solutions whose current-carrying regions are only slightly removed from the walls are similar to the analytic solutions in which the current-carrying plasmas fills the finite box. The main effect of the walls is to cause $(B_z)_{max}$ to increase past the asymptotic limit $\lambda_o = \pi/a$ of eq. (10b) as $d_{max} \to \infty$.

c) Equilibrium Solutions with Horizontal Expansion

The flux surfaces in Fig. 2a have expanded upward to a large degree with fairly large $d_{max} = 1.85$. In order to investigate equilibria with the walls farther away, allowing more room to expand horizontally as well as vertically in response to increasing d_{max}, we consider a more general class of equilibria with

$$\psi(x, 0) = \sin^{\nu}(\pi x/a) \tag{15}$$

with $\nu > 1$. For purposes of illustration we again consider solution of eq. (7), satisfying the boundary condition (19). Then,

$$\psi(x,y) = \sum_{n=1}^{\infty} A_n \sin\left(\frac{n\pi x}{a}\right) \frac{\sinh[k_n(b - y)]}{\sinh k_n b} \tag{16}$$

where $k_n = [(n\pi/a)^2 - \lambda_o^2]^{1/2}$. If $k_n^2 < 0$, hyperbolic sine is replaced by sine. Here, A_n are the Fourier sine coefficients of eq. (15). In Fig. 4, $(B_z)_{max}$, which is equal to λ_o (from $B_z = \lambda_o\psi$ and $\psi_o = 1$), is shown as a function of d_{max} for $\nu = 7$. We see that $(B_z)_{max}$ increases past π/a for $d_{max} \gtrsim 2$ but with a much smaller slope than for $d_{max} \lesssim 2$. Also plotted in Fig. 4 is the total current in the z-direction, $I_z = \int dxdy j_z = \int dxdy B_z(\psi) dB_z/d\psi$. This component of current is seen to increase quadratically for small d_{max} ($I_z \propto \lambda_o^2$) and to continue to increase for larger d_{max}. This behavior appears to be general for straight two-dimensional arcade equilibria, as will be shown with more general examples. For the equilibrium given by eq. (8) with $n = 1$, I_z is proportional to $\lambda_o^2/k_1 = \lambda_o^2/(\pi^2/a^2 - \lambda_o^2)^{1/2}$.

In Fig 5(a), we show the flux surfaces for an equilibrium with $\nu = 7$,

$$d(x) = d_o(x - a/2) \tanh^2\left[\frac{(x - x_v)}{W(a/2 - x_v)}\right] \qquad x_v < x < a/2 \tag{17a}$$

$$= 0 \qquad x < x_v \tag{17b}$$

(and again antisymmetric about x=a/2) having $x_v = 0.31$ ($\psi_v = 0.25$), $d_{max} =$

0.36, and W = 0.40. For this example, ψ_W = 0.40 which intersects the surface S at x = 0.34. The change in form between eqs. (12) and (17) [providing continuous derivative d'(x) at x_v], and the larger value of W, serve to make the solutions less sensitive to behavior near $\psi = \psi_v$. The corresponding profiles of $d(\psi)$, $B_z(\psi)$, and $\lambda(\psi)$ are shown in Figs. 5(b)-5(d). The equilibria shown in Figs. 6 and 7 have larger footpoint displacements d_{max} = 0.61 and 1.35, respectively. It is easily seen that the flux surfaces expand upward and outward as d_{max} increases.

In the example of eqs. (8), (13) and (16), and in the numerical results shown in Figs. 3 and 4, $(B_z)_{max}$ continues to increase with d_{max} approaching a limiting value or increasing depending upon whether the upward expansion of flux surfaces, and therefore further increase of $V'(\psi)$, is limited by a wall at y = b. For the examples shown in Figs. 5-7, the flux surfaces are allowed to expand horizontally as well as vertically. The effect of allowing horizontal spreading of the flux surfaces manifests itself in the graph on $(B_z)_{max}$ versus d_{max} in Fig. 8. For equilibria of the series (B) shown in Figs. 5-7, for which x_v = 0.31 and W = 0.40, there is a peak in $(B_z)_{max}$ at d_{max} = 0.35. For another related series (A) of equilibria, having x_v = 0.17 ($\psi_v = 9 \times 10^{-3}$) and W = 0.45, the peak is broader and is located near d_{max} = 0.5. The observed decrease in $(B_z)_{max}$ is related to horizontal spreading for the following reason: if no horizontal spreading occurs, as in eqs. (8), (13) and (16), B_z increases very slowly for large d_{max}, and in the case of eq. (8), has an asymptote $(B_z)_{max} \to \pi/a$. As we have discussed, this behavior is due to the fact that vertical spreading in flux surfaces, i.e. the increase in the $V'(\psi)$ term in eq. (6a), can provide the increase in d_{max} with little change in $(B_z)_{max}$. When horizontal spreading is allowed by having the photospheric flux concentrated as in eq. (15), $V'(\psi)$ can increase at a rate faster than d_{max}, giving a decrease in $(B_z)_{max}$. For the case of Fig. 4 described by eqs. (15) and (16), this effect cannot occur. Mathematically, this is simply traced to the fact that if $\lambda_0 = (B_z)_{max}$ is prescribed in eq. (7), then the solutions are unique, and therefore only one value of d_{max} is possible for each λ_0. Physically, this appears to arise from the fact that for $\psi_v = 0$, the outer surfaces spread out horizontally even for very small d_{max}, when $(B_z)_{max}$ is increasing rapidly. Thus, it appears that, in order for $(B_z)_{max}$ to attain a peak and decrease thereafter, a certain amount of potential

flux, or at least a profile having $\lambda(\psi) \to 0$ as the wall is approached, is required to separate the current-carrying region and the fixed walls so that the flux surfaces can spread out against a "soft" wall when the displacement is large. Nevertheless, for even larger d_{max}, $(B_z)_{max}$ must again begin to increase, when the expansion of flux surfaces is arrested by the walls. This effect may be beginning to occur for $d_{max} \gtrsim 1$ in Fig. 8. However, this effect is due to the unphysical boundaries. We expect that $(B_z)_{max}$ will continue to decrease in the absence of such boundaries.

In our iteration scheme to solve the G-S equation for specified d_{max} (Appendix B), the outer iteration loop described by eq. (12) converges very rapidly near the peak in $(B_z)_{max}$ and beyond, because the solutions have a relatively weak dependence upon d_{max}. However, the inner loop given by eq. (B1) does not noverge for solution near and past this in $(B_z)_{max}$. This is because $B_z(\psi)$ is specified in the inner loop as an intermediate step and the peak corresponds to a bifurcation in this case. Although such bifurcations are not physical as discussed in Secs. I and IIb, they have mathematical and numerical significance for our iteration scheme. In general, an iteration as in eq. (B1) is expected to converge for one class of solutions (with smaller d_{max}) and diverge for the other class (with larger d_{max}). We overcome the divergence problem by renormalizing $B_z(\psi)$ in the inner loop iterations [that is, changing $(B_z)_{max}$ with no change in the profile $B_z(\psi)/(B_z)_{max}$] in order to conserve the total z-current $I_z = \int dxdy B_z dB_z/d\psi$. This is a simple operation because I_z scales as $(B_z^2)_{max}$. From Fig. 4, we see that I_z increases much more rapidly with d_{max} than $(B_z)_{max}$ for the solution given by eq. (16). In fact, it is found that I_z increases for all solutions even when $(B_z)_{max}$ decreases. With this prescription in which I_z rather than $(B_z)_{max}$ is held fixed during the iteration process, there is no bifurcation. When this method is employed, the inner loop iterations are always found to converge.

For $d_{max} = 0.36$ (Figs. 5a - 5d), the region of strong shear in footpoint displacement is $0.31 < x < 0.34$, or equivalently $0.26 < \psi < 0.40$. In this region, $B_z(\psi)$ [Fig 5(c)] deviates significantly from linearity. Note that $\lambda(\psi) = dB_z/d\psi$ is not constant (Fig. 5d), decreasing to zero as ψ decreases. This behavior is consistent with the general properties discussed in Sec. IIIa. Closer to the center, $x > 0.34$ and $\psi > 0.40$, B_z is fairly linear in ψ, although λ shows a slight peaking at the center. Since $j = \lambda(\psi)B$ for these equilibria, this indicates a peaking of the current

density relative to the solutions of the form eqs. (8), (13) and (16). In Fig. 6, for a larger footpoint displacement with d_{max} =0.61, this tendency appears to be somewhat more pronounced. Although not evident in Fig. 6(b), Figure 6c shows a sharp drop-off in λ in the shear region $0.26 < \psi < 0.40$, a further peaking near the center ($\psi > 0.8$) and a plateau in between. For a still larger footpoint displacement $d_{max} = 1.35$ (Fig. 7c), this tendency is even more pronounced, with $\lambda(\psi)$ having a rather narrow peak for $\psi > 0.9$, sharp drop-off in the shear region $0.26 < \psi < 0.40$, and a valley around $\psi = 0.7$. The current density $j_z = B_z dB_z/d\psi = \lambda B_z$ is quite peaked; its value at the center $x = a/2$, $y = 0$ ($\psi = 1$) is 65 (in normalized units), compared to a considerably lower value of 10 at $\psi = 0.7$. That is, in a sense, solutions with increasing d_{max} exhibit a considerable amount of peaking in the current density. Nevertheless, we will show below that the peaking in j_z at the center with increasing d_{max} does not lead to formation of current sheets. Moreover, the current density perpendicular to the photosphere $j_y = \lambda B_y = -\lambda \partial\psi/\partial x$ is proportional to $\sin^6(\pi x/a)\cos(\pi x/a)\lambda(\psi)$. Because B_y is small near $x = a/2$ ($\psi = 1$), the peak in λ also does not correspond to a large peaking of j_y.

In Fig. 9, λ_{max}, the maximum value of $\lambda(\psi)$, is shown as a function of d_{max}. This maximum occurs at $\psi = \psi_o$ for all cases. Recall that $\lambda_{max} = \lambda_o$ is identical to $(B_z)_{max}$ for solutions eqs. (8), (13), and (16). For the equilibria of Fig. 9, however, there are qualitative differences. Note that λ_{max} begins to flatten for increasing d_{max}, at $d_{max} \simeq 0.2$ for series B and at $d_{max} \simeq 0.4$ for series A while $(B_z)_{max}$ peaks at $x \simeq 0.35$ and $x \simeq 0.5$, respectively. However, in both cases λ_{max} continues to increase, unlike $(B_z)_{max}$. It seems likely that λ_{max} may have a peak with respect to d_{max} for larger values of x_v and/or W. However, for the present parameters, the proximity of the wall causes the slow increase in λ_{max} for $d_{max} \gtrsim 0.4$. This behavior shows further the lack of any physical meaning to the "bifurcations" in Fig. 8.

We now consider the peaking in $\lambda(\psi)$ and $j_z(\psi)$ in more detail. In Fig. 10, we show the maximum current density j_z as a function of d_{max}. For solutions of eq. (7) (for example, eqs. [8], [13], and [16]), j_z is proportional to λ_o^2 [$j_z = \lambda_o^2\psi$; see eq.(7)]. We see that for series A and B, j_z and λ are seen to have similar behavior; j_z increases rapidly for $d_{max} \lesssim$

0.35 (series B) and for $d_{max} \lesssim 0.50$ (series A), the same regions for rapid increase in Figs. 8 and 9. Also, j_z continues to increase, but much more slowly, for larger values of d_{max}. The slow increase of j_z for $d_{max} \gtrsim 0.5$ appears to be due to the proximity of the wall. We also expect that $(j_z)_{max}$ might decrease with d_{max} for larger x_v and/or W. At the same time, the profile of $j_z = \lambda B_z$ continues to narrow so that the total j_z current in the peak region decreases. In Fig. 11, we show the total z-current I_z is shown for series A and B. It is observed to increase quadratically for $d_{max} \lesssim 0.1$ and monotonically for all d_{max} (as noted above.) However, I_z does not increase as rapidly for large d_{max} as in Fig. 4. The important points to note are (i) that the peak current density j_z is always found to increase at a very slow rate with respect to d_{max}, giving a decrease in the total j_z current in the peak region. Concurrently, (ii) the total current I_z increases rapidly with d_{max}, so that the fraction of the total current I_z carried by the peak decreases very rapidly with d_{max}.

We point out that the single-valuedness of the graphs in Figs. 8-11 is due to the fact that a single solution is found when $d(\psi)$ is specified. We take this as empirical evidence that these solutions are unique. Therefore, any other physical quantity such as the total magnetic energy will also be single-valued. It has also been found that the total magnetic energy of a linear dipole field can be well fitted with a logarithmic dependence on footpoint shear (Klimchuk, Sturrock, and Yang 1988).

As we have discussed in Sec. IIc and Appendix B, finite β equilibria with entropy prescribed can be computed in essentially the same manner. In Fig. 12 we show results with $d_{max} = 0$ (i.e. $B_z = 0$) as a function of the maximum entropy s_{max}. As suggested by the analogy between eqs. (B4) and (B5), the form of $s(\psi)$ is chosen to be $[d(\psi)]^{1/2}$, where $d(\psi)$ is the footpoint displacement form factor of eq. (17). Fig. 12a, we show the dependence of p_{max} versus s_{max} for $x_v = 0.31$ and $W = 0.40$, the same choices as in curve B in Fig. 8. We have used zero footpoint displacement since the results of Zwingmann (1987) show that this is the case with the strongest degree of bifurcation when pressure is specified. We see that p_{max} is a well-behaved, single-valued function of s_{max}. For very small s_{max}, increasing s_{max}, i.e., the internal energy content, predominantly leads to a linear increase in p_{max}. This curve has a broad maximum around

$s_{max} \simeq 0.3$; increasing s_{max} in this region leads to expansion of the structure in such a way that p_{max} remains nearly unchanged. For $s_{max} \gtrsim 0.4$, increasing s_{max} is predominantly accomplished by expansion of the structure and the pressure in fact decreases. This behavior is similar to that of $(B_z)_{max}$ versus d_{max} (see Fig. 8). The flux surfaces are similar to those shown in Figs. 5a, 6a, 7a. The overall behavior of equilibria with respect to variation of s_{max} is generally similar to that with respect to d_{max} with no remarkable differences. We note that Fig. 7 of Zwingmann (1987), which corresponds to a solution on the upper branch of the W (energy) versus λ_p (a measure of pressure) curve, shows apparent formation of an O-point. Such an equilibrium cannot evolve from configurations without O-points via ideal MHD motions. Mathematically, such O-points will not occur when $d(\psi)$ or $s(\psi)$ is prescribed because these quantities are specified only on the range $0 < \psi < \psi_0$ and the occurence of an O-point indicates the existence of surfaces with $\psi > \psi_0$, the maximum flux value specified on S. The occurence of O-points when $B_z(\psi)$ is specified has also been found by Birn, Goldstein, and Schindler (1978).

In Fig. 12b, we show the total axial current I_z and the peak current density $j_z(x=a/2, y=0)$. As the entropy increases, the current density $j_z = dp/d\psi$ becomes peaked at the center, as in the case of increasing the footpoint displacement. However, the total current again increases at a faster rate with respect to s_{max} than the current in the peak region ($x = a/2$), so that the fraction of the current associated with the peak decreases relative to I_z as s_{max} increases. No remarkable differences appear to exist between specifying d_{max} and specifying s_{max}, consistent with the mathematical similarity apparent in the formulations in eqs. (6a) and (6c). Note that p_{max} and I_z are well-behaved, single-valued functions of s_{max}. Thus, the total energy, which is the sum of the magnetic energy and internal energy ($\propto p$) integrated over the volume, is single-valued, exhibiting no bifurcations.

IV. Discussion

The basic physical mechanism behind the expansion of the flux surfaces as d_{max} or s_{max} is increased is relatively simple. The force-free equilibrium condition $\underline{j} \times \underline{B} = 0$ can be written as $(j_p B_z - j_z B_p) = 0$, where j_p is the transverse (x,y) component. For a force free equilibrium, $j_p B_z \sim dB_z^2/d\psi$ is an upward force if B_z monotonically increases in ψ. In an imaginary two-step process (Sec. IIb), if the footpoint displacement is increased, at first with no change in the flux surfaces [no change in $\psi(x,y)$, B_p or j_z], B_z must increase. However, the plasma will be out of equilibrium and will expand upward under $j_p B_z$ until force balance is achieved again. This expansion will occur with d_{max} conserved in the limit of infinitely conducting photosphere, which means that the B_z flux between any two flux surfaces will be conserved. This expansion process will then necessarily decrease B_z. In the new equilibrium, B_z may be greater than or less than that of the initial equilibrium, depending on whether the initial increase of B_z dominates the subsequent decrease of B_z. There is a simple circuit analogy to this process. As we have seen in the discussion following eq. (6), $d(\psi)$ is proportional to the axial flux between two nearby flux surfaces. Also, $B_z(\psi)$ is essentially the total transverse current between the flux surface labelled by ψ and that labelled by ψ_v (see the discussion after eq. [3]). By eq. (6a), $V'(\psi)$ (which is a property only of the geometry of the flux surfaces) can therefore be identified as the inductance relating transverse current to axial flux. In the first step of the imaginary two-step process above, when the photospheric motion takes place (d_{max} is increased) with the geometry held fixed, we have $LdI/dt = V_o$. The voltage V_o is proportional to the tangential electric field on the photospheric surface $E_x = v_z B_y$. In the second step, the geometry and current change, conserving flux $d(LI)/dt = 0$. For small d_{max}, the process is completed primarily by increasing the current with little change in inductance; for large d_{max}, the inductance increases by an amount sufficiently large that the current must decrease.

A similar argument applies to the pressure. In thermal equilibrium, the thermal input and radiative loss between any two flux surfaces, say, ψ_1 and ψ_2, are balanced. If, for example, the heating rate increases, the pressure "initially" (i.e., before relaxation to equilibrium) increases.

Then, in approaching equilibrium, the flux surfaces ψ_1 and ψ_2 will both expand under ∇p in such a way as to decrease the pressure, by adiabatic decompression (assuming that MHD time scales are shorter than radiative or thermal time scales). During this process, if expansion dominates, then the new equilibrium pressure will be lower than that of the initial equilibrium. The imaginary two-step process described in Sec. IIb and above is helpful not only for conceptualization but for predicting the response of the coronal plasma to a source of heat that occurs on a faster time scale than the nominal heating and radiative loss mechanisms.

The scenario for which entropy rather than pressure should be specified assumes that the photosphere does not act as a source of material or energy. This can achieved if thermal conduction along the field lines between the corona and the photospheric or subphotospheric regions is negligible on the MHD time scale for relaxation to equilibrium, or equivalently, if the magnetic field in the arcade is large enough and the coronal density small enough that the Alfven time scale is much shorter than the time scale for parallel thermal conduction in the photosphere. This argument also assumes that radiation is negligible on the Alfven time scale. On the other hand, if the radiation is dominant, and the plasma is isothermal, the mathematical formulation is essentially identical to the adiabatic case (but with adiabatic index $\gamma = 1$.) In our computation, we have also assumed that the arcade length scales are short compared with the coronal gravitational scale height $2kT_c/mg$, so that $p = p(\psi)$ in the corona. This is only for convenience, and is not critical, especially if $\beta = 2p/B^2$ is small. (The photospheric scale height $2kT_p/mg$, on the other hand, is assumed to be small. This is important in order to be able to specify footpoint displacement. This is consistent with T_p being much less than T_c.) On the other hand, suppose one attempts a justification for specifying coronal pressure based on the dominance of photospheric processes by specifying the photospheric pressure $p(\psi,0)$. Accordingly, assume that an increased photospheric pressure is imposed with no changes in the flux surfaces, as in the imagined two-step process discussed above. At this step in the process, the increased coronal pressure is given by eq. (4b). Then, the pressure $p(\psi,y)$ will subsequently decrease as the system relaxes to equilibrium. There does not seem to be a reasonable conservation law, one based upon an energy equation for the plasma, in

which the pressure in the corona $p(\psi,y)$ given by eq. (4b) can be specified. Using this interpretation, we conclude that bifurcations with respect to prescribing pressure do not correspond to a physical loss of equilibrium.

The effect of expansion of the flux surfaces and the effect upon the curves in Figs. 8 and 12a can be understood better by the following scaling argument. First, consider the force free case $s(\psi) = p(\psi) = 0$. For arcades that are free to expand upward but are constrained in the horizontal direction (e.g., eqs. [8] and [13]; also Fig. 2a), the Grad-Shafranov equation (5a) implies in the large d_{max} limit that $B_z \sim \psi/a$, independent of the height h of the flux surfaces. From eq. (6a), we have $d = B_z V'$ so that, for large h, $V' \sim ah/\psi$, $d \sim (\psi/a)(ah/\psi)$ and $h \sim d$. On the other hand, if the plasma is free to expand in both directions, its width will be of the same order as its height h for large h and the G-S equation gives $B_z \sim \psi/h$. Using $V' \sim h^2/\psi$, we again obtain $d \sim (\psi/h)(h^2/\psi) \sim h$. This in turn implies $B_z \sim \psi/d$ for large d. This exact scaling is not observed in the results of Fig. 8 for two reasons. First, the effect of the proximity of the wall is probably non-negligible for $d_{max} \gtrsim 1.0$ in Fig. 8. Second, such a scaling argument cannot include the effects of profile changes, e.g., the peaking in the λ profile seen in Fig. 7c. Nevertheless, this scaling does illustrate the general features of the results observed.

A similar scaling law can be obtained if entropy is specified with $d(\psi) = B_z(\psi) = 0$. If only vertical expansion is allowed, then $p \sim \psi^2/a^2$ (from the G-S equation) and, using $s = pV'^{\gamma}$, we obtain $s \sim (\psi^2/a^2)(ah/\psi)^{\gamma}$ for large h, or $s \sim h^{\gamma}$. For two-dimensional expansion, we obtain $p \sim \psi^2/h^2$ and $s \sim (\psi^2/h^2)(h^2/\psi)^{\gamma} \sim h^{2(\gamma-1)}$. We then find the scaling $p \sim s^{-1/(\gamma-1)} \sim s^{-3/2}$. Expressing these results in terms of an equivalent footpoint displacement $\delta \equiv (2s)^{1/2}$ and an equivalent $B_z' \equiv (2p)^{1/2}$ as suggested by eqs. (14a) and (14b), we find $B_z' \sim \delta^{-3/2}$. Again, these scalings are in qualitative agreement with the results of Fig. 12a.

The results presented in Figs. 5-11 and Fig. 12b have a bearing on the development of a so-called "open field configuration". This open field configuration is defined as the potential solution having the same boundary condition on the flux $\psi(x,o)$ but necessarily having a sheet current along $\psi = \psi_o$. It has been stated (Barnes and Sturrock 1972; Yang, Sturrock, and Antiochos 1986; Aly 1984,1985) that the field approaches such a

configuration as the footpoint displacement increases. The current is conjectured to become entirely concentrated into the sheet. As noted in the discussion of Fig. 7c, the transverse components of the current density do not become peaked in space as d_{max} increases. Also the magnitude of the transverse current density j_p scales as λ_{max} with increasing d_{max} and thus increases slowly for large d_{max}. Furthermore, the total transverse current is proportional to $(B_z)_{max}$ and is found to decrease as d_{max} is increased. The other component of current density $j_z = B_z dB_z/d\psi$ becomes peaked near $\psi = \psi_o$ (see the discussion of Fig. 7c). However, the peak of j_z at $x = a/2$ increases slowly for large d_{max} (Fig. 10). (The slow increase in the peak value of j_z for $d_{max} \gtrsim 0.5$ is again attributable to the influence of the walls.) Furthermore, the total j_z current in the peak region decreases. On the other hand, the total z-current I_z increases at a considerably faster rate than the peak current density. We conclude that the peak in j_z near $\psi = \psi_o$ contributes a rapidly <u>decreasing</u> fraction of the total current I_z as d_{max} increases, and therefore sheet currents with progressively narrower current profiles carrying the bulk of the current do not occur. The increase in I_z appears to be due to the same cause as the increase of I_z for eq. (8) for which $I_z \propto \lambda_o^2/(\pi^2/a^2 - \lambda_o^2)^{1/2}$, namely that the equilibrium continues to expand, with nearly uniform current density filling the space. We conclude that increasing the footpoint displacement does indeed cause the flux surfaces to expand but that the resulting equilibrium approaches a configuration with finite current density (j_z) and increasing total current I_z but no concentration of the current into sheets.

In the present paper, we have adopted the conventional approach that the footpoints of magnetic field lines are tied to the infinitely conducting and massive photosphere and have found no bifurcations (i.e., no loss of equilibrium) with respect to physically specifiable quantities. In this scenario, all the flux associated with the arcade is contained in the corona. If the photosphere is assumed to have finite conductivity and finite mass, then the fluxes can extend below. In a recent paper, Chen (1989) studied the behavior of "toroidal" current loops in which the current was assumed to be closed in or below the photosphere. In this work, a circuit parameter $\varepsilon \equiv \Phi_p/\Phi_T = L_p/L_T$ was found to play a role in determining the stability behavior of a loop, where Φ_p (L_p) is the flux

(inductance) in the corona enclosed by the loop and Φ_T (L_T) is the total flux (inductance) including the flux structure below the photosphere associated with the loop. Thus, the quantity ε parametrizes the subphotospheric flux/current structure relative to what is above the photosphere. In this model, the infinitely conducting and massive photosphere assumption corresponds to the $\varepsilon = 1$ limit. In this limit, loops are found to be stable. If, on the other hand, the subphotospheric flux is large enough (ε less than some critical value ε_{cr}), then a loop can be unstable to major radial expansion, leading to a wide range of motion and magnetic energy dissipation. In the present linear arcade model, too, it is possible that if the fluxes are allowed to extend below the photosphere, loss of equilibrium or instabilities may occur.

V. Summary

A study of two-dimensional MHD equilibrium of linear coronal arcades has been presented. An iterative method has been used to solve the Grad-Shafranov equation with prescribed footpoint displacement $d(\psi)$ or entropy $s(\psi)$. This method involves, as an intermediate mathematical step, the prescription of B_z and $p(\psi)$. A modification of the method has been developed to compute equilibria through purely mathematical bifurcation points which can occur when axial field B_z and pressure are prescribed in the intermediate steps. Sequences of equilibria have been computed with $d(\psi)$ or $s(\psi)$ specified. No multiple solutions exist if $d(\psi)$ is specified, consistent with the suggestion of Jockers (1978) and in agreement with the recent result of Zwingmann (1987). We have also shown that no multiple solutions exist if the entropy $s(\psi)$ is specified. The entropy, like the pressure, is a measure of the internal energy of the plasma. Generally, if the entropy is specified, then the pressure cannot be specified and vice versa. In the limit in which the arcade plasma can be assumed to be adiabatic, then the entropy rather than the pressure is physically specifiable. In this case, the pressure-based bifurcations do not indicate the possibility of an eruptive process. We have described physical conditions under which the entropy may be specified, and discussed the difficulty in posing a physically meaningful situation in which the pressure is specifiable. Our results indicate that increasing footpoint displacement and entropy increases the magnetic energy of an arcade but not the magnetic free-energy to drive eruptive processes in the corona.

We have also investigated the formation of the so-called open field configuration and formation of sheet current (e.g., Barnes and Sturrock 1972; Aly 1984,1985; Yang, Sturrock and Antiochos 1986) and found that the profile of the current density j_z indeed becomes more peaked with increasing footpoint displacement but that the total j_z current in the peak region decreases as the total current I_z increases, so that a rapidly <u>decreasing</u> fraction of current is carried by the current peak at the center ($x = a/2$). Based on our solutions, especially Figs. 10,11 and 12(b), we expect no sheet current formation (i.e., concentration of current at $x = a/2$) to takes place as a result of increasing footpoint displacement.

ACKNOWLEDGMENTS

We wish to thank P. Sturrock, S. Antiochos and E. Zweibel for stimulating discussions. This work was supported by the Office of Naval Research.

REFERENCES

Aly, J.J., 1984 Ap. J., 283, 349.

Aly, J.J., 1985 Astron. Astrophys., 193, 19.

Antiochos, S. K. 1989, in "Solar and Stellar Flares: Poster Papers", eds. B. M. Haisch and M. Rodono, publ. Oss. Astrfis. Catania, No. ____, (in press).

Barnes, C. and Sturrock, P. 1972, Ap. J., 174, 659.

Birn, J., Goldstein, H., and Schindler, K. 1978, Solar Phys., 57, 81.

Birn, J. and Schindler, K., 1981, in Solar Flare Magnetohydrodynamics, ed. E. Priest, Gordon and Breach, N.Y.

Chen, J. 1989, Ap. J., March, (in press).

Chodura, R. and Schluter, A. 1981, J. Comput. Phys.,41,68.

Drake, J. F., Hassam, A. B., and G. Van Hoven 1988, Plasma Preprint UMLPR #88-044, University of Maryland.

Grad, H., Hu, P. N., and Stevens, D. C. 1975, Proc. Nat. Acad. Sci USA,72,3789.

Heyvaerts, J., Lasry, J. M., Schatzman, M., and Witomsky, P. 1982, Astr. Ap., 111, 104.

Heyvaerts, J. and Priest, E. R. 1984, Astr. Ap., 137, 63.

Jockers, K. 1978, Solar Phys., 56, 37.

Keller, H. B. 1977, in P. Rabinowitz (ed.), Applications of Bifurcation Theory, New York: Academic Press.

Klimchuk, J., Sturrock, P. and Yang, W. H. 1988, Center for Space Science and Astrophysics Report CSSA-ASTRO-87-17 (submitted to Ap. J.).

Low, B. C. 1977, Ap. J., 212, 234.

Low, B. C. 1982, Ap. J., 263, 952.

Low, B. C. and Wolfson, R. 1988, Ap. J., 324, 574.

Lundquist, S. 1951, Phys. Rev., 83, 307.

Mikic, Z., Barnes, D.C., and Schnack, D.C. 1988, Ap. J., 328, 830.

Parker, E. N. 1972, Ap. J., 174, 499.

——— 1983, Ap. J., 264, 642.

Priest, E. R. 1988, Ap. J., 328, 848.

Sturrock, P. A., ed. 1980, Solar Flares, Boulder: Colorado Associated University Press.

van Ballegooijen, A. A. 1985, Ap. J., 298, 421.

Wu, S.T., Bao, J.J., Tandberg-Hanssen, E., 1987, Space Science Laboratory Preprint Series No. 87-147.

Xue, M. L. and Chen, J. 1983, Solar Phys., 84, 119.

Yang, W.H., Sturrock, P.A., and Antiochos, S.K. 1986 Ap. J., 309, 383.

Zweibel, E. and Li, H.-S. 1987, Ap. J., 312, 423.

Zwingmann, W., 1987, Solar Phys, 111, 309 .

Appendix A

As an aside, we note that Clebsch variables have been used by other authors in specifying footpoint displacements. That is, the total field is written as

$$\underline{B} = \nabla\alpha \times \nabla\beta,$$

where $\alpha = \psi$ and $\beta = z - f(x,y)$. Writing $f(x,y) = \Theta(x,y)d_o(\psi)$ and using eq. (1a), we find

$$\underline{B}\cdot\nabla\Theta = B_z(\psi)/d_o(\psi)$$

$$\Theta = \frac{B_z(\psi)}{d_o(\psi)} \int \frac{ds}{B},$$

with an indefinite integral along the field line. If Θ is required to increase by unity in integrating from one footpoint to the other, we obtain, from eq. (6a), that $d_o(\psi) = d(\psi)$. Therefore, specification of $f(x,0)$ at one footpoint (e.g. where $B_n > 0$) is equivalent to specifying $d(\psi)$.

Appendix B

The computational method we employ is to start with a trial $B_z(\psi)$. For brevity, we begin with the case p = 0. We iterate eq. (5a) by solving

$$L\psi_{k+1} \equiv \nabla^2\psi_{k+1} = R(\psi_k), \tag{B1}$$

where $R(\psi) = - B_z(\psi)dB_z/d\psi$. Given ψ_k, a standard Poisson solver is used to solve eq. (B1) for ψ_{k+1}. Formally, this can be expressed as $\psi_{k+1} = L^{-1}[R(\psi_k)]$. It is helpful to introduce a relaxation parameter r and iterate according to $\psi_{k+1} = rL^{-1}[R(\psi_k)] + (1-r)\psi_k$. The convergence properties of the inner loop iteration $\psi_k(\underline{x}) \rightarrow \psi_{k+1}(\underline{x})$ depend on the bifurcation properties of eq. (5a) with the trial function $B_z(\psi)$. In order to carry out the iteration past the mathematical bifurcation points arising from specifying B_z as an intermediate step, it is necessary to take the further step of renormalizing $B_z(\psi)$ such that the total axial current I_z remains fixed during successive iterations.

For a given footpoint displacement $d(\psi)$, we integrate along the field lines to compute $V'(\psi)$, defined in eq. (6b). We then compute $B_z(\psi)$ from eq. (6a) with a relaxation parameter ρ such that

$$B_z^{new}(\psi) = \rho d(\psi)/V'(\psi) + (1 - \rho)B_z{}^{old}(\psi). \tag{B2}$$

The method of inner-outer loop iteration is best summarized in a flow chart as follow. First, we specify the footpoint displacement $d(\psi)$. We then

1) guess a solution to eq. (B1) by giving $B_z(\psi)$ and $\psi(x,y)$, and compute the total axial current I_z;

2) iterate eq. (B1) with a (inner-loop) relaxation parameter r. If d_{max} is on the right side of the mathematical bifurcations (e.g., for $d_{max} >$ 0.35 for the B-series equilibria of Fig. 8), renormalize $B_z(\psi)$ at each

iteration so that I_z remains unchanged for the series of "inner loop" iterations. There is no bifurcation with respect to I_z;

3) compute $V'(\psi)$ (eq. [6b]) for these solutions to eq. (5);

4) update $B_z(\psi)$ by eq. (B2) with a second (outer-loop) relaxation parameter ρ, and return to step 2.

For small footpoint displacement, $V'(\psi)$ is insensitive to changes in footpoint displacement because ψ is the potential solution to lowest order. In this case, the outer loop iteration (B2) (with relaxation parameter ρ = 1) converges rapidly. For larger footpoint displacement, $V'(\psi)$ becomes quite sensitive, but in practice it is found that the iteration oscillates if it diverges, and therefore a positive relaxation parameter ρ (with ρ decreasing with d_{max}) guarantees convergence, provided the iteration process is properly chosen if mathematical bifurcation with B_z specified occurs as described above. This is discussed further in Sec. IIc for specific examples. This method of inner and outer loop iterations generally converges very rapidly if the correct relaxation parameters are chosen. However, it often requires an accurate first guess for $\psi(x,y)$ if footpoint displacement is large. Therefore, we generally find solutions by varying parameters from one run to the next, starting with small footpoint displacement.

A similar scheme is used to include pressure when the entropy $s(\psi)$ is prescribed. The analogue to eq. (B1) is $R(\psi) = -dp/d\psi$ and $p(\psi)$ is renormalized to keep I_z fixed during inner loop iterations, as discussed in Sec. IV. Using eq. (6c), the analog to eq. (B2) is

$$p^{new}(\psi) = \rho' s(\psi)/V'(\psi)^{\gamma} + (1 - \rho')p^{old}(\psi). \qquad (B3)$$

Since the right hand side of the G-S equation (5a) is $-(d/d\psi)[p(\psi) + B_z(\psi)^2/2]$, the prescriptions for computing $B_z(\psi)$ and $p(\psi)$, and their effects on the final solutions, are quite similar. This is most easily seen if we rewrite eqs. (6a) and (6c) as

$$\frac{1}{2} B_z(\psi)^2 = \frac{1}{2} d^2(\psi)/V'(\psi)^2 \qquad \text{(B4)}$$

and

$$p(\psi) = s(\psi)/V'(\psi)^{\gamma}. \qquad \text{(B5)}$$

In fact, if it were not for the rather insignificant difference between $\gamma = 5/3$ and 2, there would be a formal identification $(1/2)B_z(\psi)^2 \leftrightarrow p(\psi)$ and $(1/2)d(\psi)^2 \leftrightarrow s(\psi)$. [Similar statements hold for the isothermal plasma, in which the analogue of eq. (B5) is $\gamma = 1$ with $s(\psi)$ replaced by $M'(\psi)$.] Because of this similarity, the iteration scheme eq. (B3) has essentially identical properties as eq. (B2), but with somewhat different optimum relaxation parameters in the outer loop.

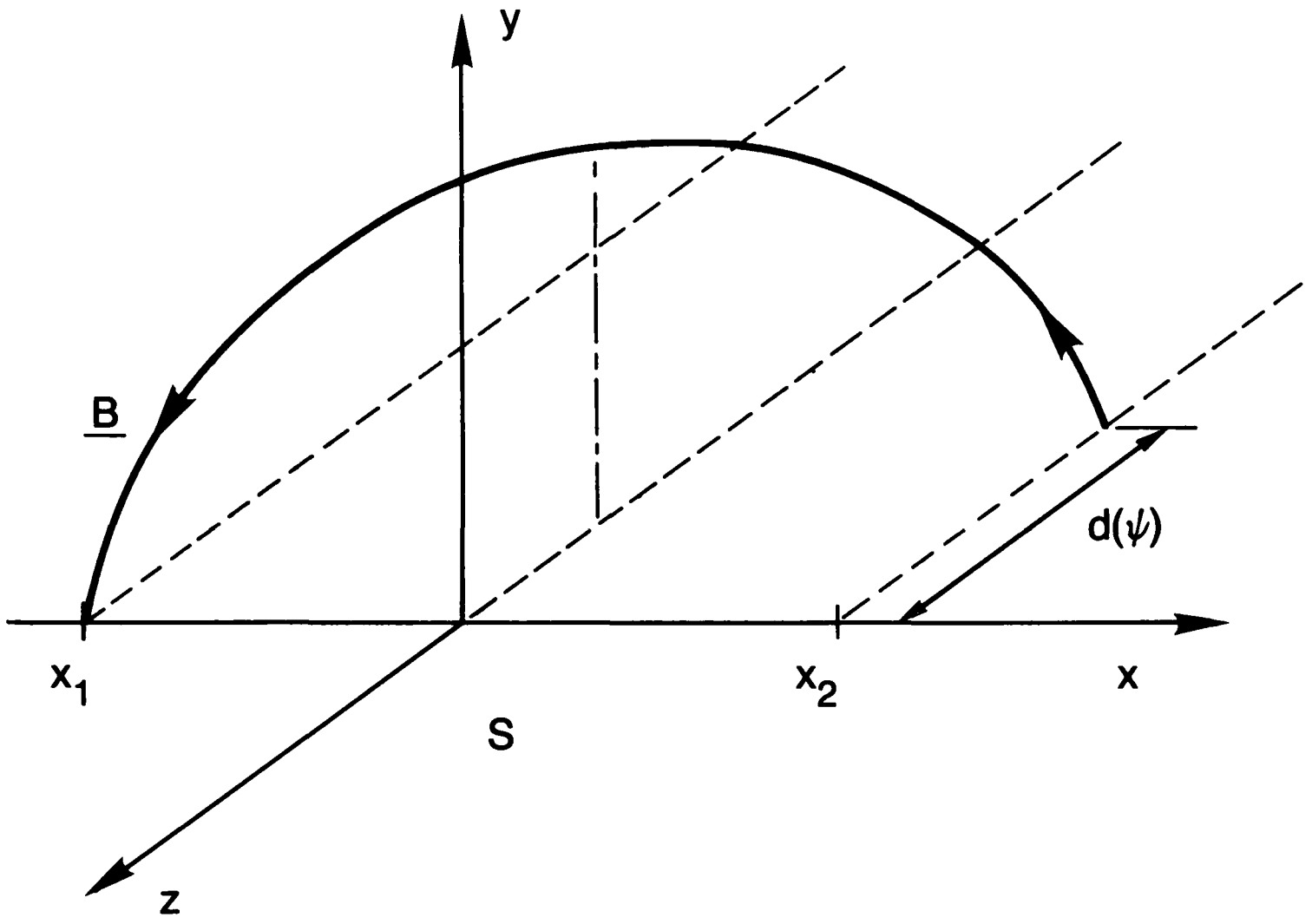

Fig. 1 — Schematic diagram of an arcade geometry. A representative magnetic field line labelled by ψ is shown with the footpoints displaced by $d(\psi)$. A field line has an "axial" component along the z-direction and a "transverse" perpendicular to z.

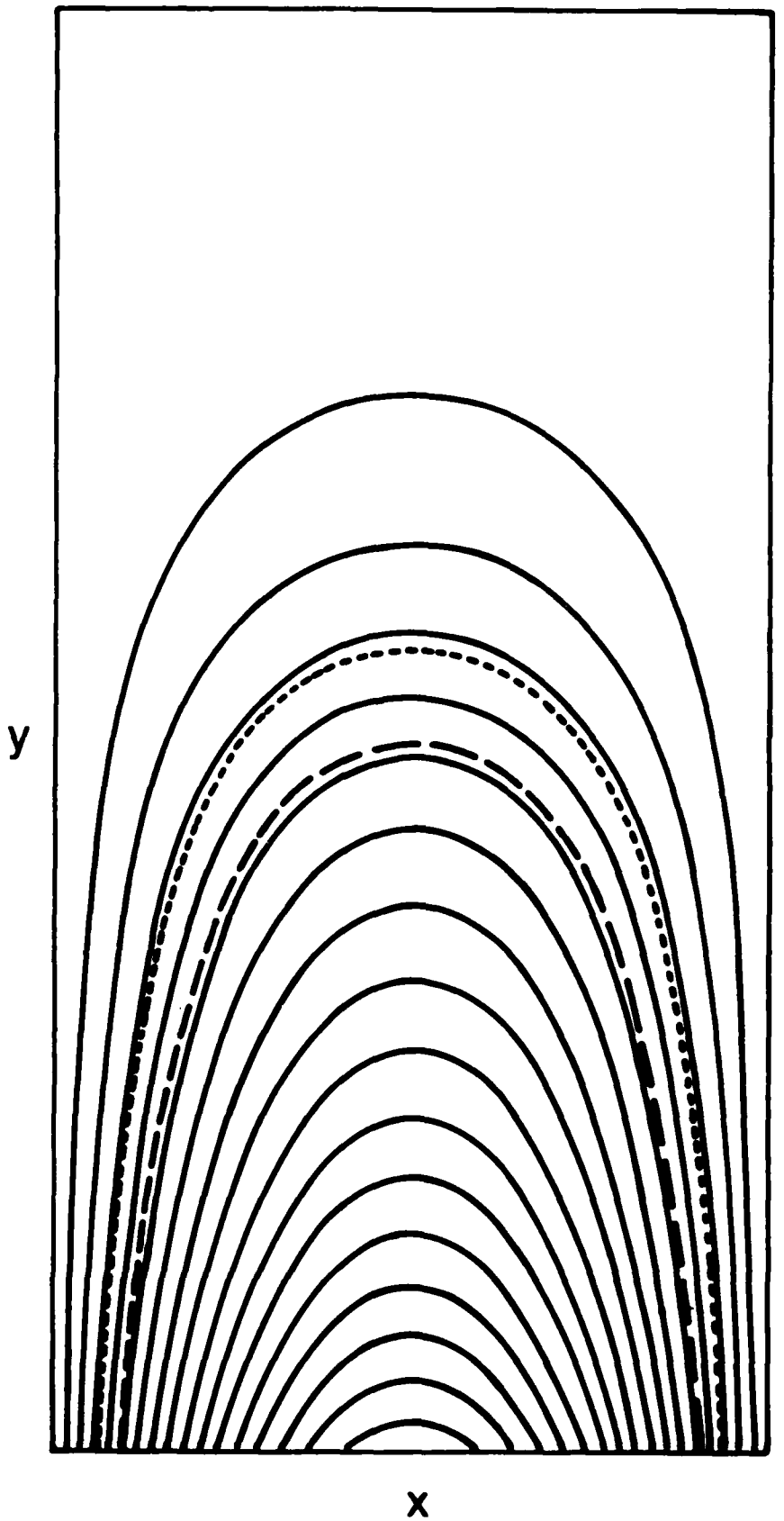

Fig. 2 — A force-free arcade for $d(\psi)$ given by Eq. (16) and $\psi(x,0) = \sin(\pi x/a)$. A relatively small amount of potential flux $\psi_v = 0.195$ surrounds the current-carrying plasma. (a) Flux (ψ) surfaces. (b) Footpoint displacement versus x. (c) B_z versus ψ. (d) $\lambda = dB_z/d\psi$

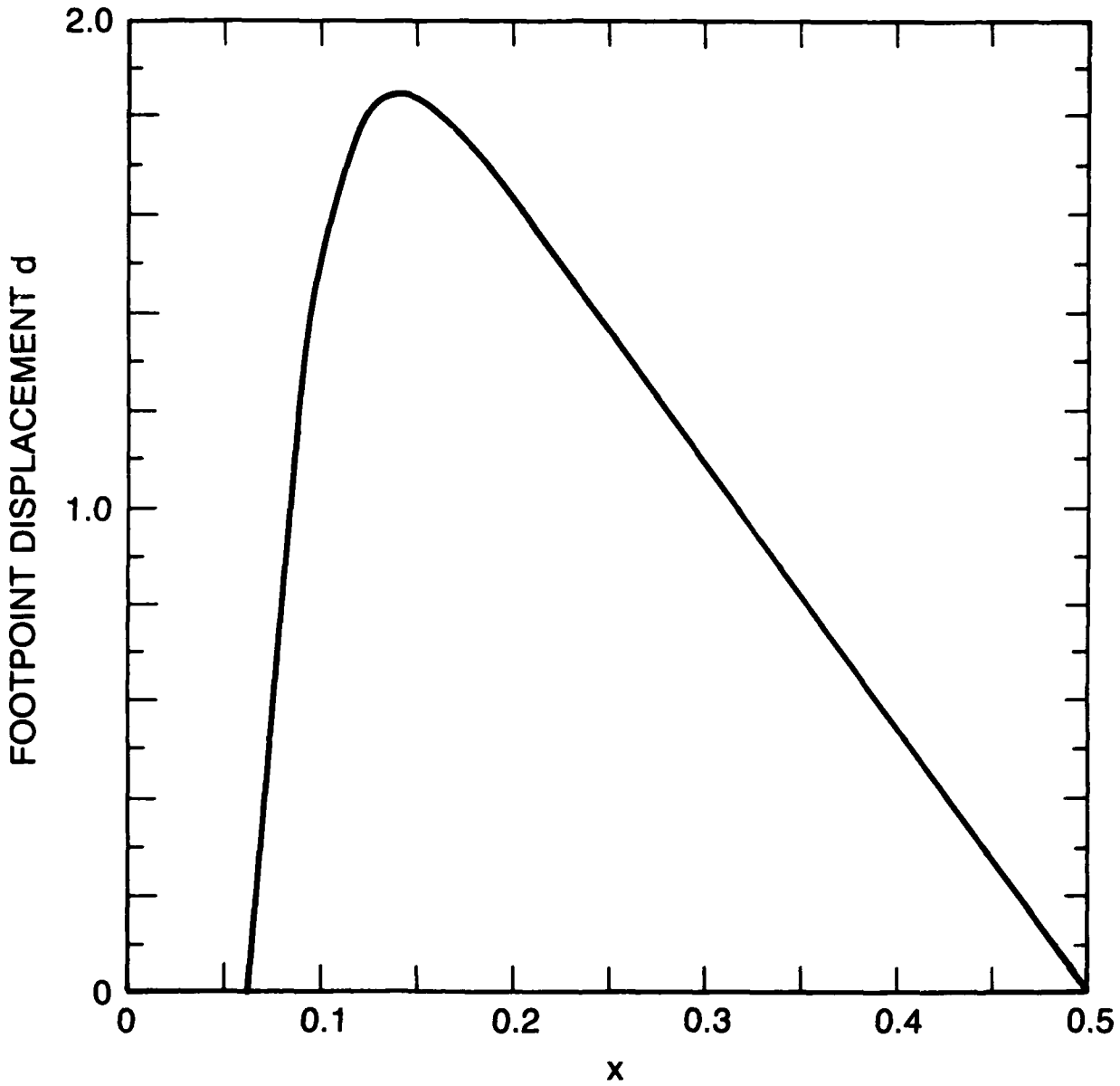

Fig. 2 (Continued) — A force-free arcade for $d(\psi)$ given by Eq. (16) and $\psi(x,0) = \sin(\pi x/a)$. A relatively small amount of potential flux $\psi_v = 0.195$ surrounds the current-carrying plasma. (a) Flux (ψ) surfaces. (b) Footpoint displacement versus x. (c) B_z versus ψ. (d) $\lambda = dB_z/d\psi$

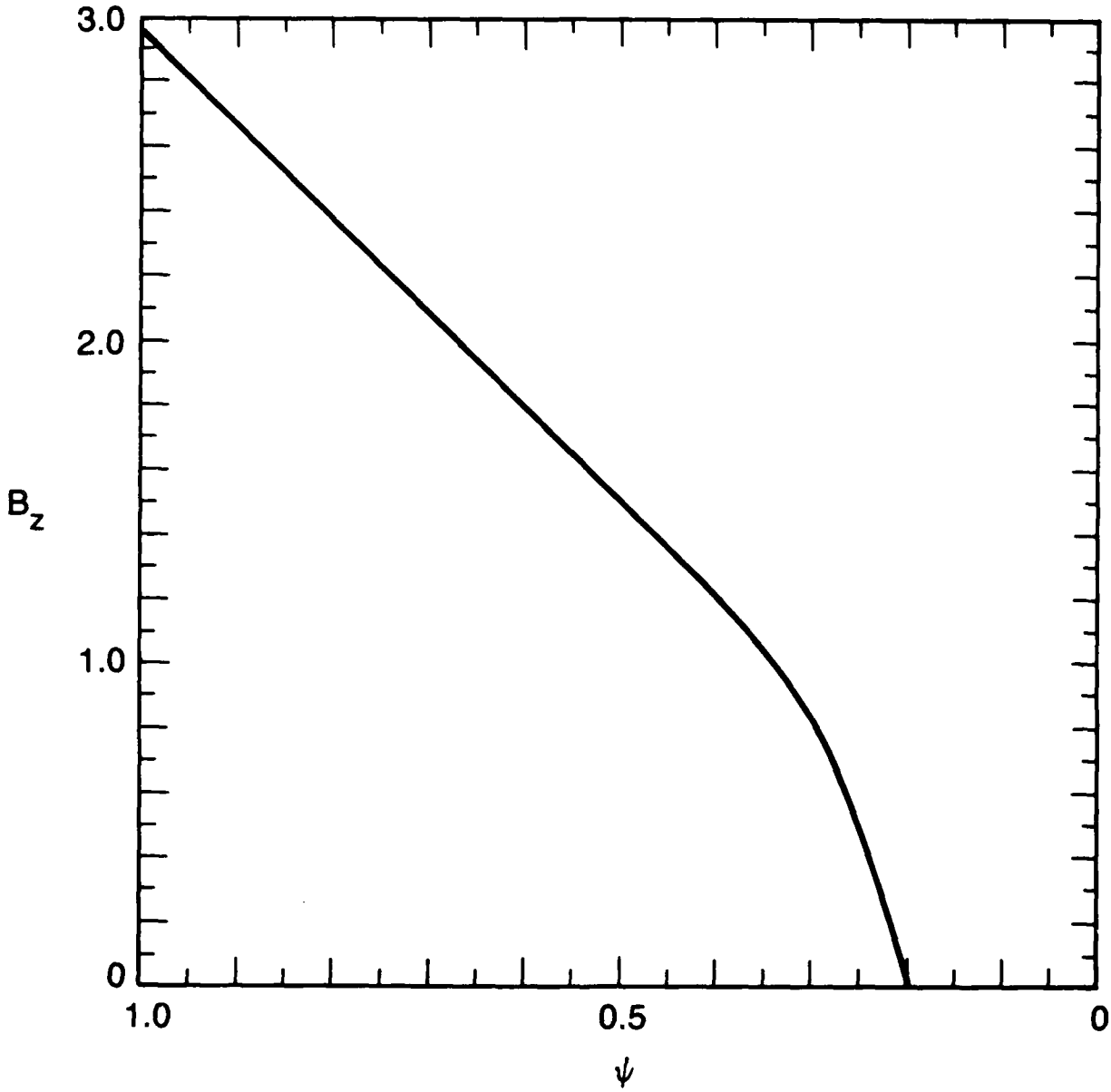

Fig. 2 (Continued) — A force-free arcade for $d(\psi)$ given by Eq. (16) and $\psi(x,0) = \sin(\pi x/a)$. A relatively small amount of potential flux $\psi_v = 0.195$ surrounds the current-carrying plasma. (a) Flux (ψ) surfaces. (b) Footpoint displacement versus x. (c) B_z versus ψ. (d) $\lambda = dB_z/d\psi$

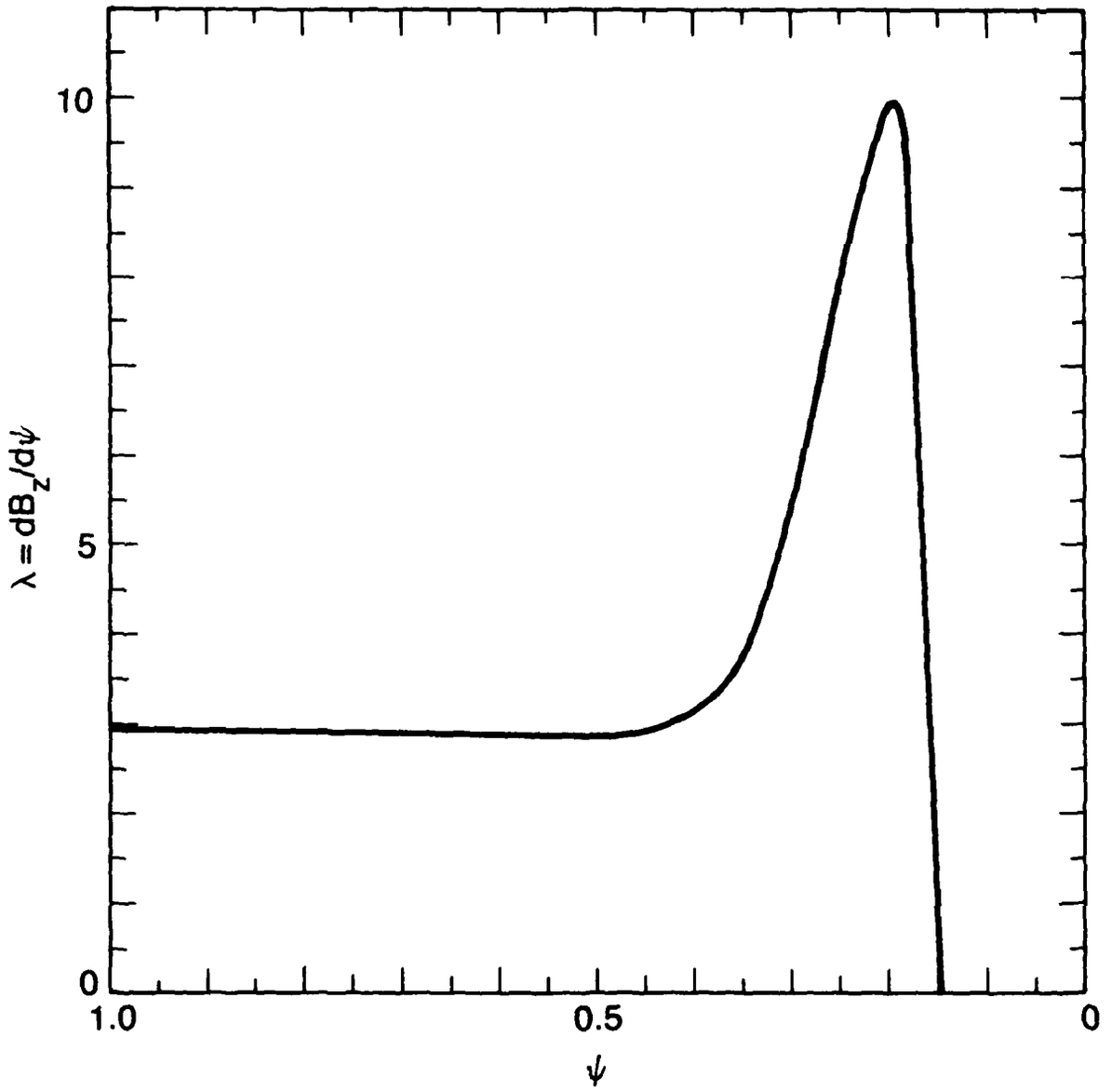

Fig. 2 (Continued) — A force-free arcade for $d(\psi)$ given by Eq. (16) and $\psi(x,0) = \sin(\pi x/a)$. A relatively small amount of potential flux $\psi_v = 0.195$ surrounds the current-carrying plasma. (a) Flux (ψ) surfaces. (b) Footpoint displacement versus x. (c) B_z versus ψ. (d) $\lambda = dB_z/d\psi$

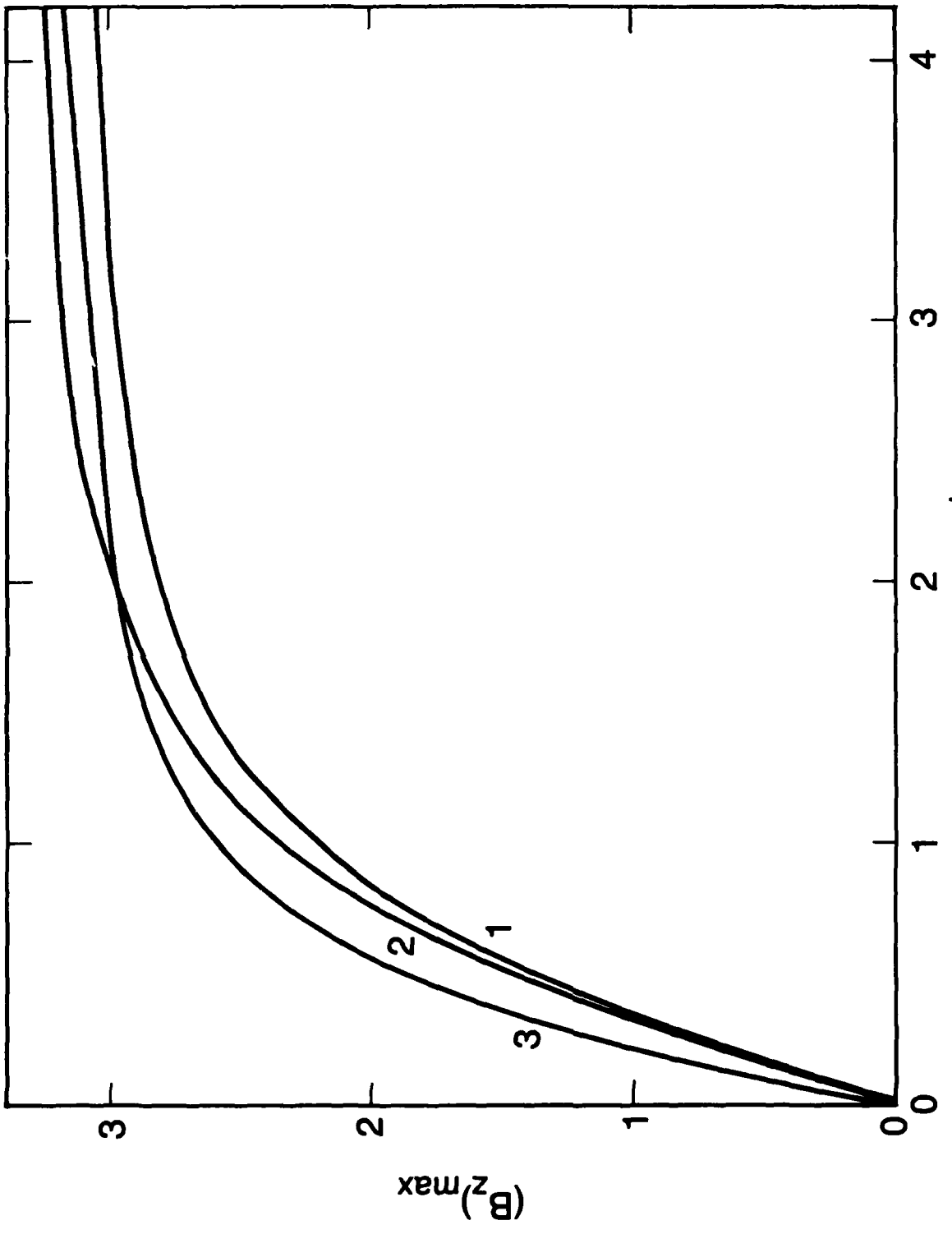

Fig. 3 — $(B_z)_{max}$ versus d_{max}. Curve 1 corresponds to equilibrium given by Eq. (8) and curve 2 to equilibrium given by Eqs. (17) and (18). Curve 3 describes the numerical equilibrium with parameters given as in Fig. 2.

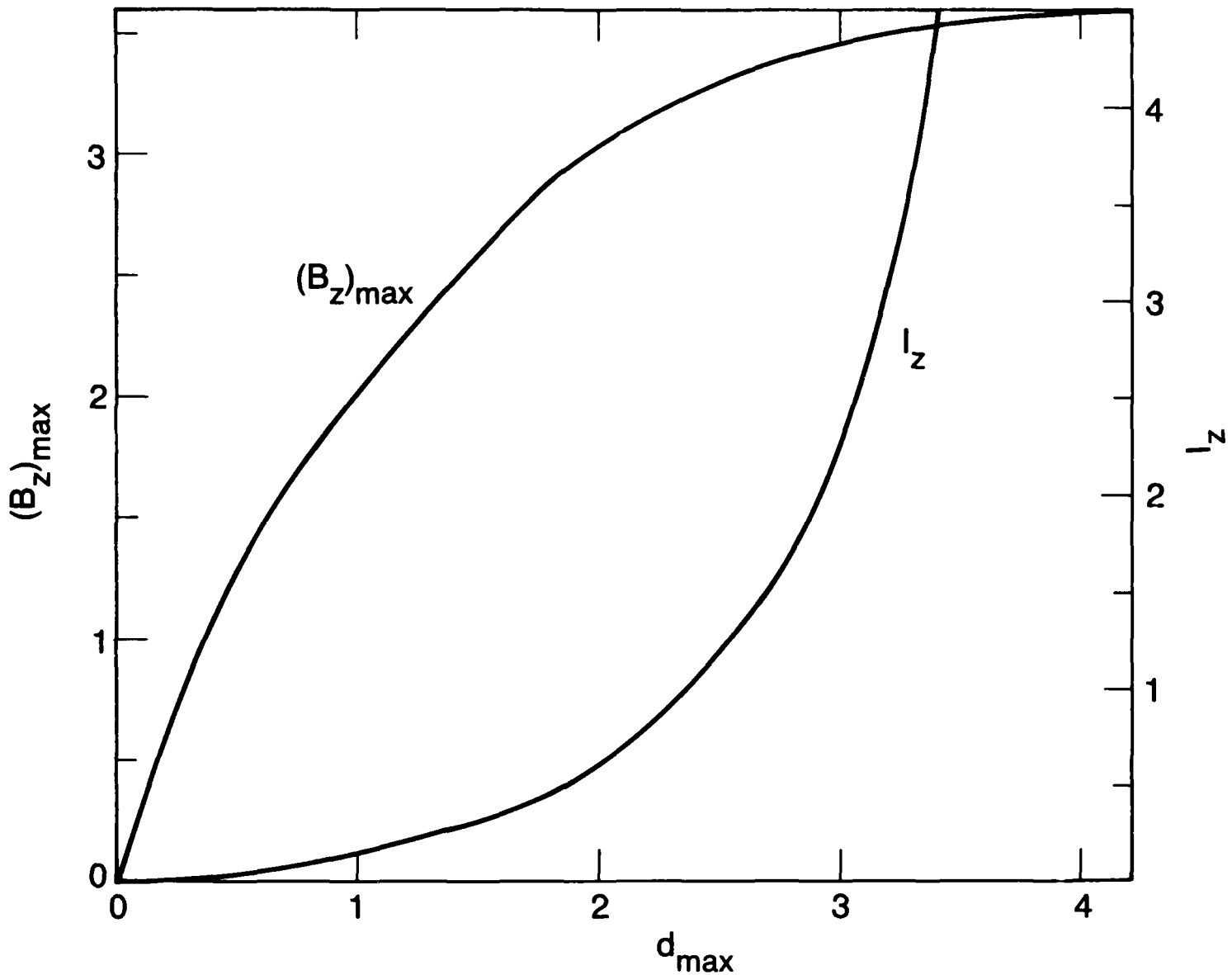

Fig. 4 — $(B_z)_{max}$ and the total current I_z as functions of d_{max} for the equilibrium analytically given in Eqs. (19) and (20) with $\nu = 7$.

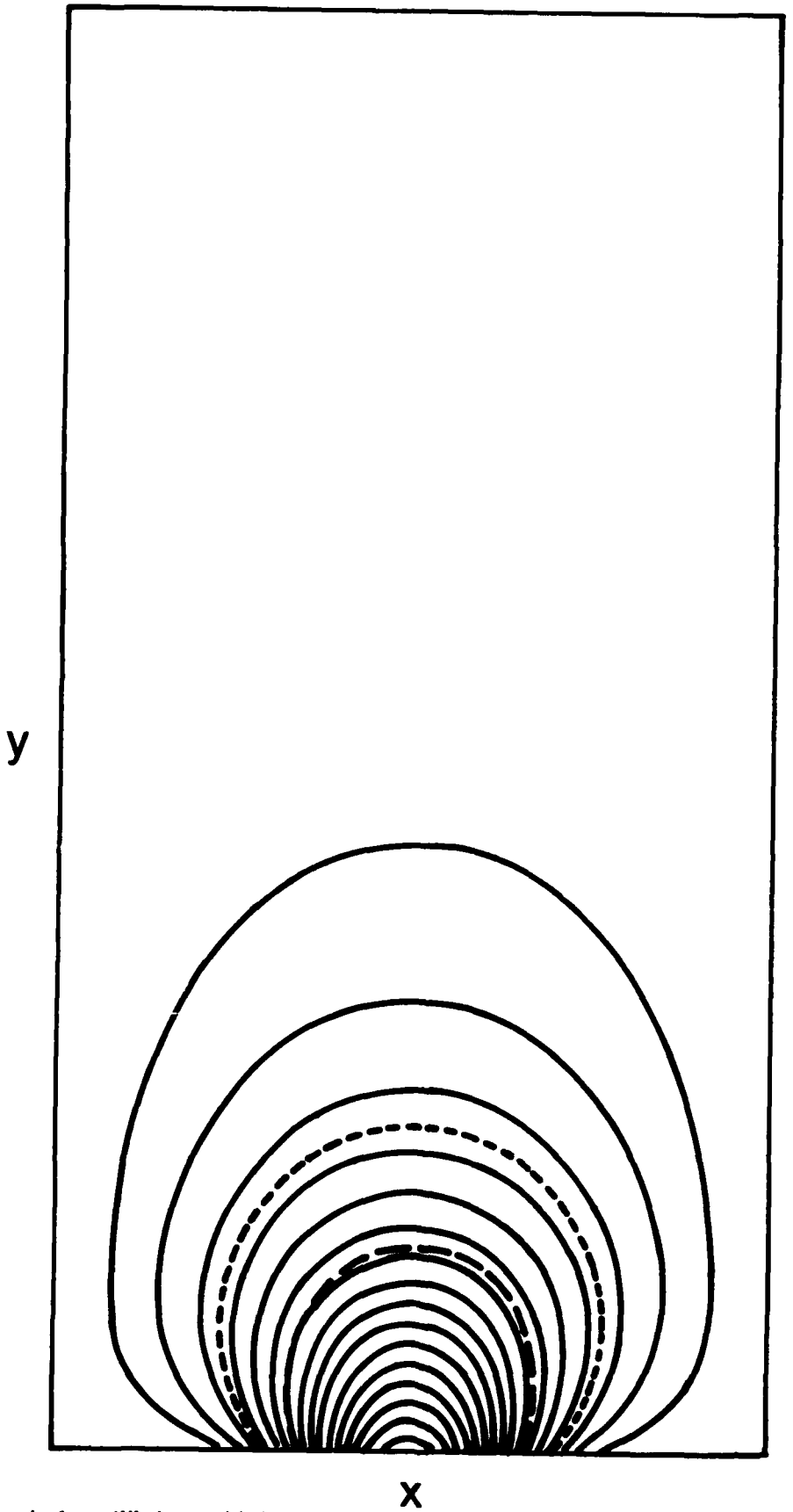

Fig. 5 — Numerical equilibrium with boundary condition given by Eq. (19) for $\nu = 7$ and with footpoint displacement given by Eq. (21). The current-carrying region is surrounded by a relatively large amount of flux $\psi_v = 0.25$ ($x_v = 0.31$), W = 0.40, and $d_{max} = 0.36$. (a) Flux surfaces. (b) Footpoint displacement versus x. (c) B_z versus ψ. (d) λ versus ψ.

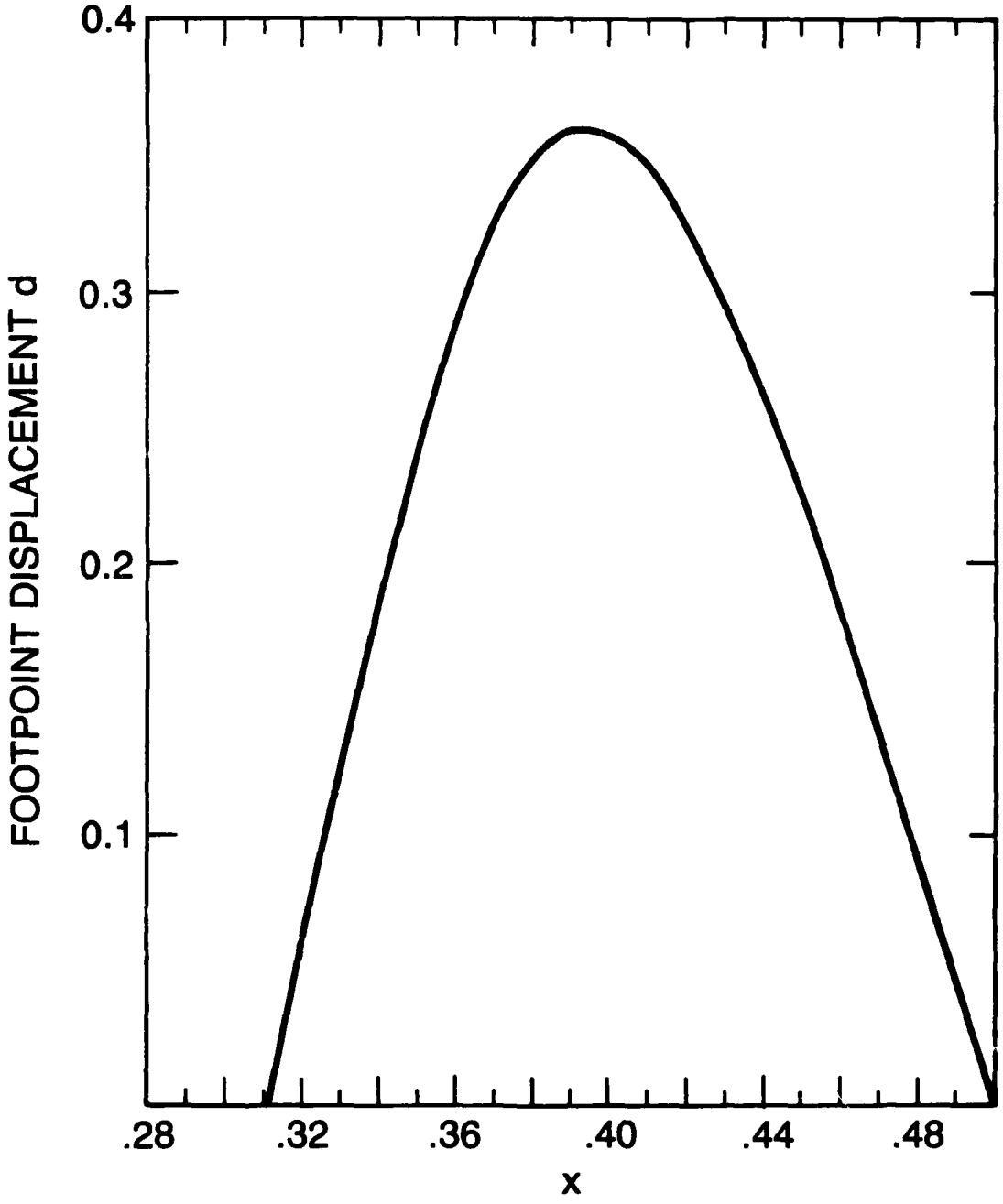

Fig. 5 (Continued) — Numerical equilibrium with boundary condition given by Eq. (19) for $\nu = 7$ and with footpoint displacement given by Eq. (21). The current-carrying region is surrounded by a relatively large amount of flux $\psi_v = 0.25$ ($x_v = 0.31$), W = 0.40, and $d_{max} = 0.36$. (a) Flux surfaces. (b) Footpoint displacement versus x. (c) B_z versus ψ. (d) λ versus ψ.

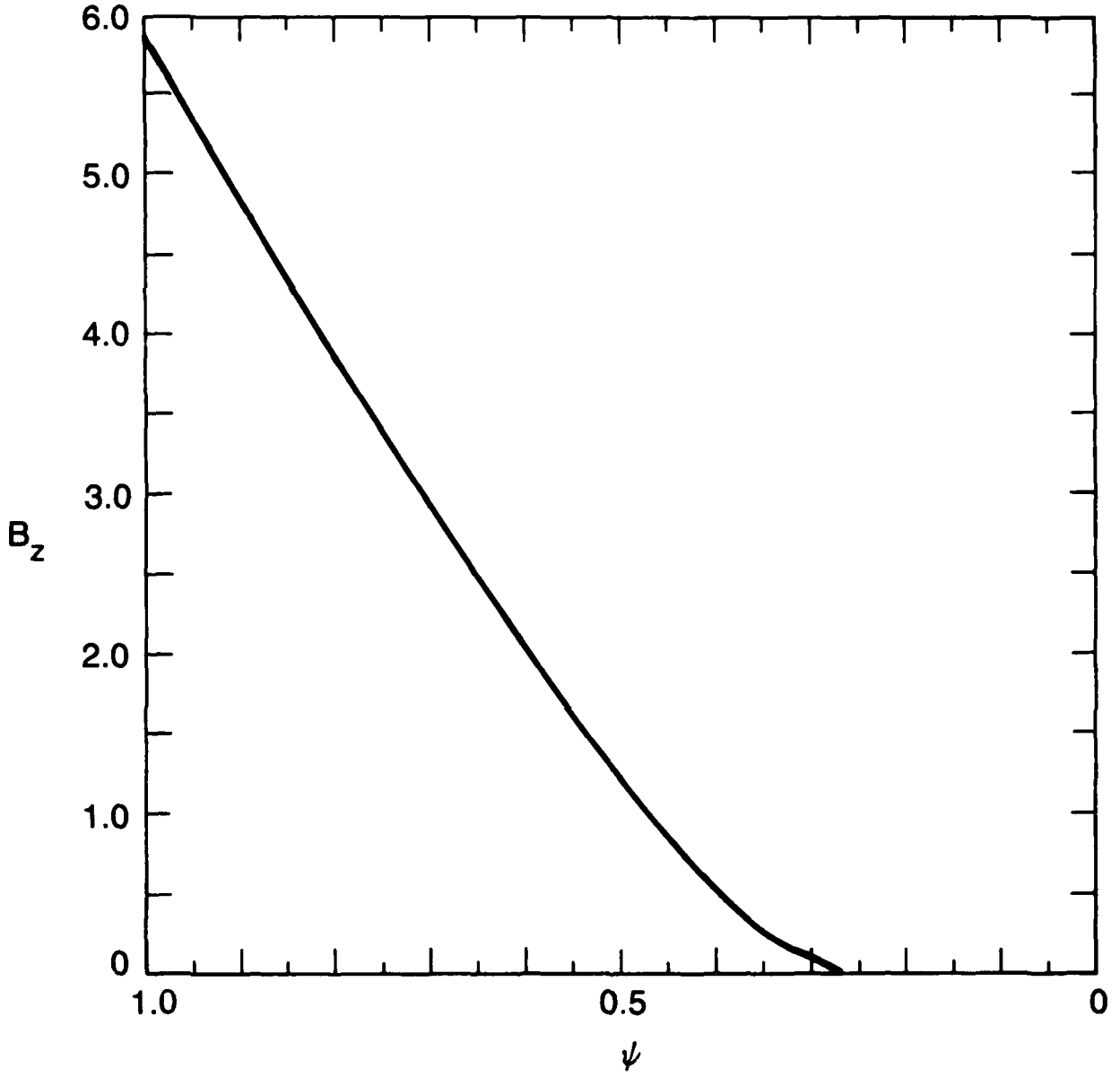

Fig. 5 (Continued) — Numerical equilibrium with boundary condition given by Eq. (19) for $\nu = 7$ and with footpoint displacement given by Eq. (21). The current-carrying region is surrounded by a relatively large amount of flux $\psi_v = 0.25$ ($x_v = 0.31$), W = 0.40, and $d_{max} = 0.36$. (a) Flux surfaces. (b) Footpoint displacement versus x. (c) B_z versus ψ. (d) λ versus ψ.

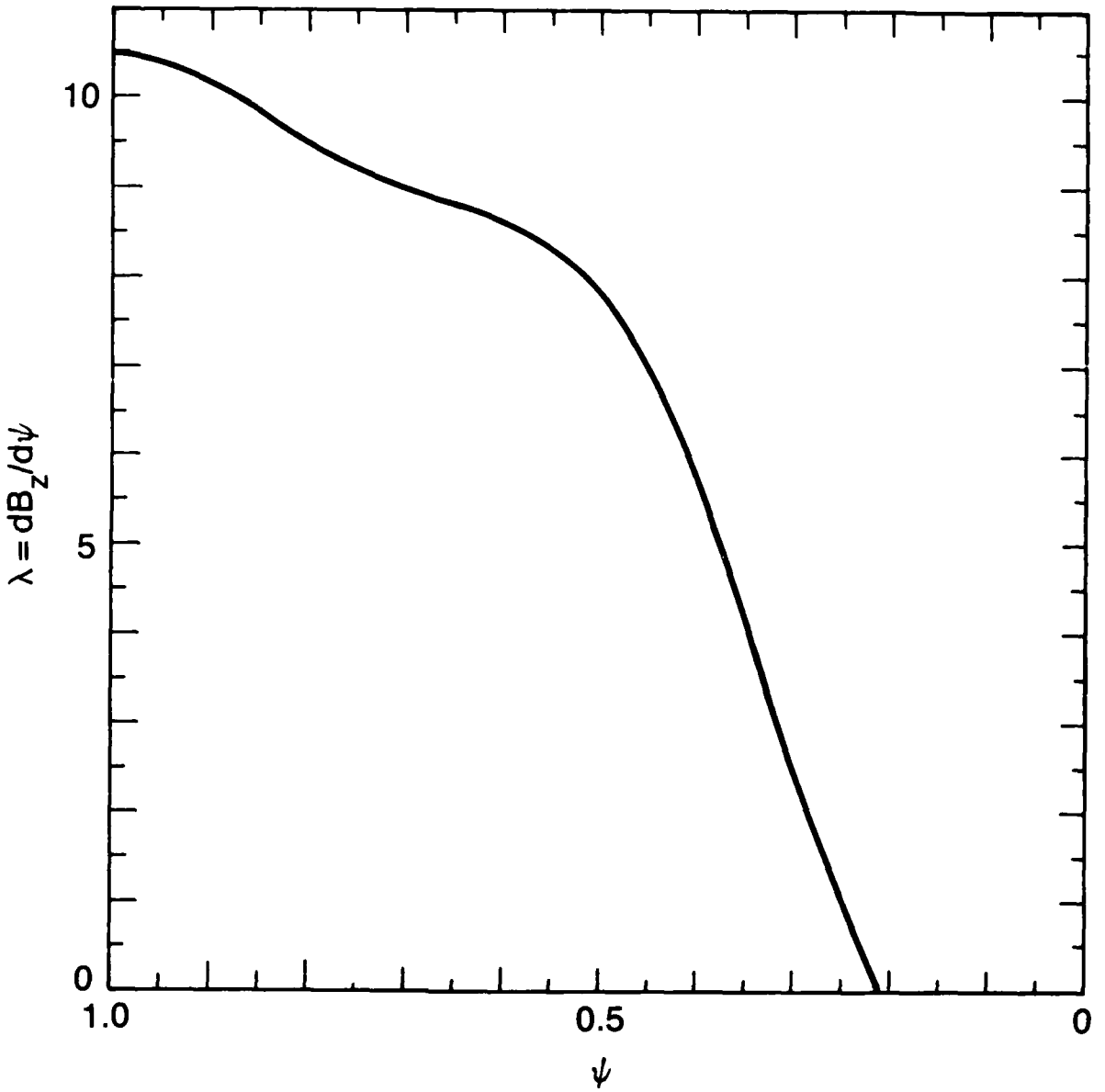

Fig. 5 (Continued) — Numerical equilibrium with boundary condition given by Eq. (19) for $\nu = 7$ and with footpoint displacement given by Eq. (21). The current-carrying region is surrounded by a relatively large amount of flux $\psi_v = 0.25$ ($x_v = 0.31$), W = 0.40, and $d_{max} = 0.36$. (a) Flux surfaces. (b) Footpoint displacement versus x. (c) B_z versus ψ. (d) λ versus ψ.

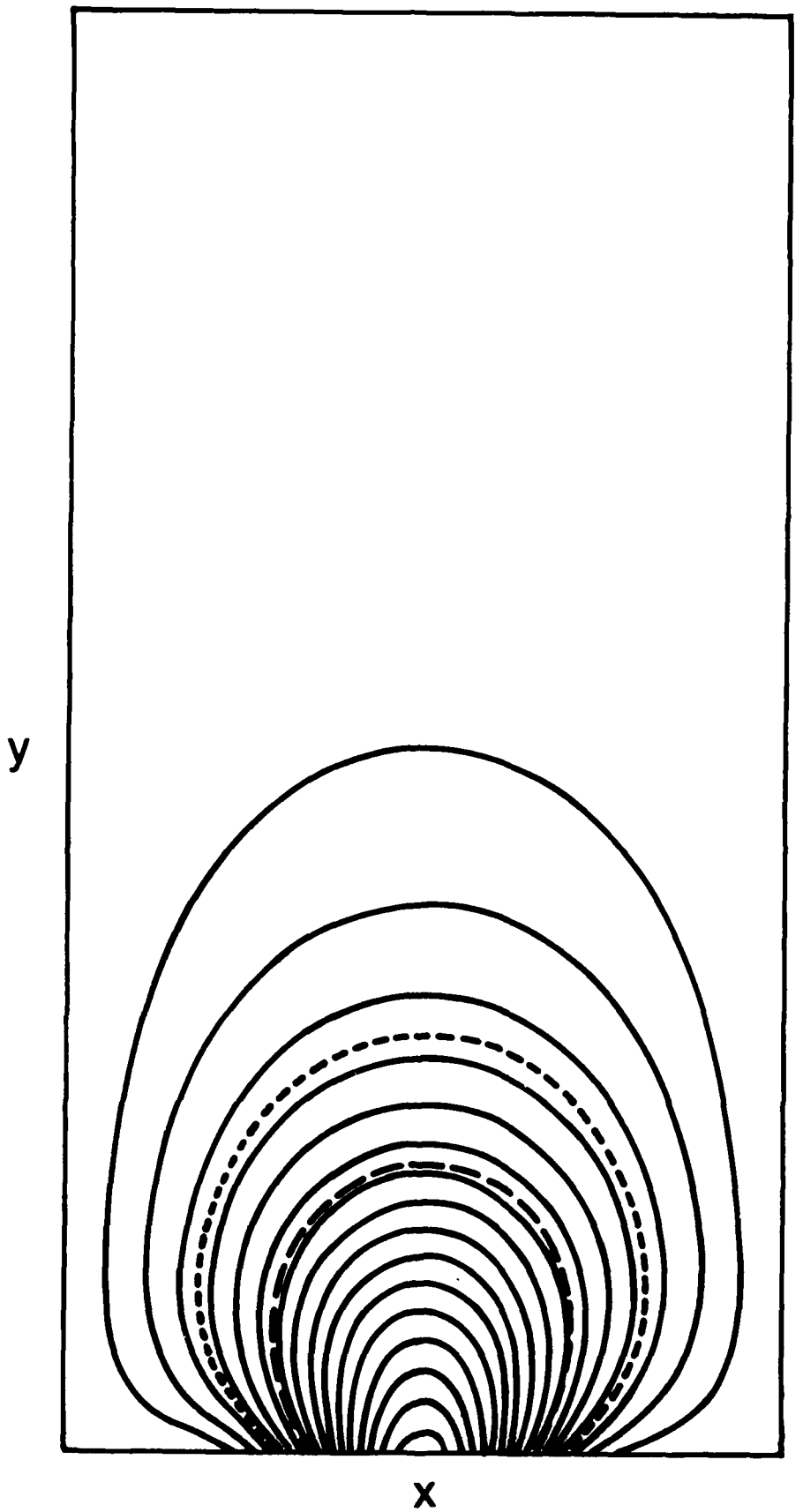

Fig. 6 — Equilibrium with parameters as in Fig. 5 except $d_{max} = 0.61$.

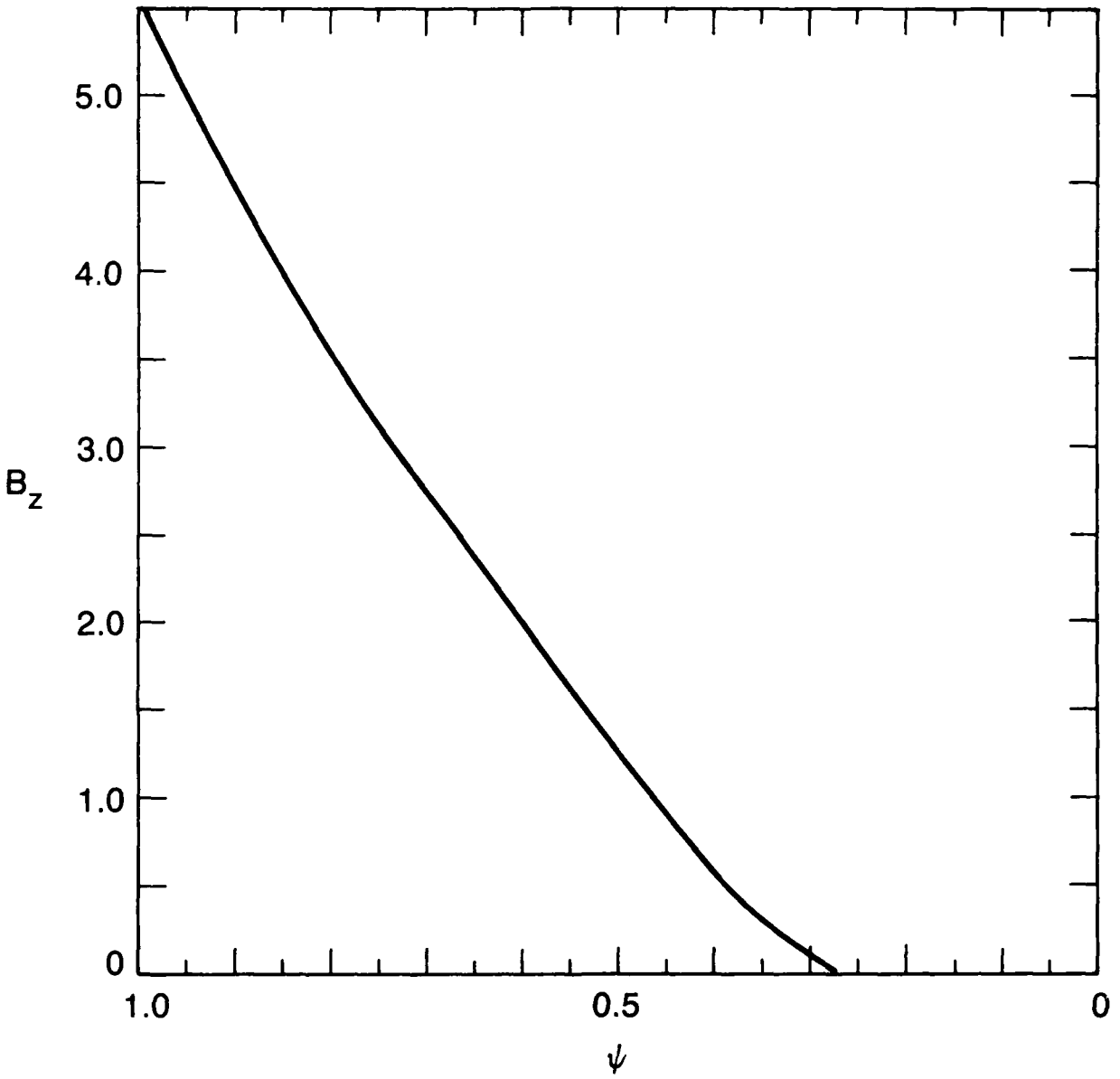

Fig. 6 (Continued) — Equilibrium with parameters as in Fig. 5 except $d_{max} = 0.61$.

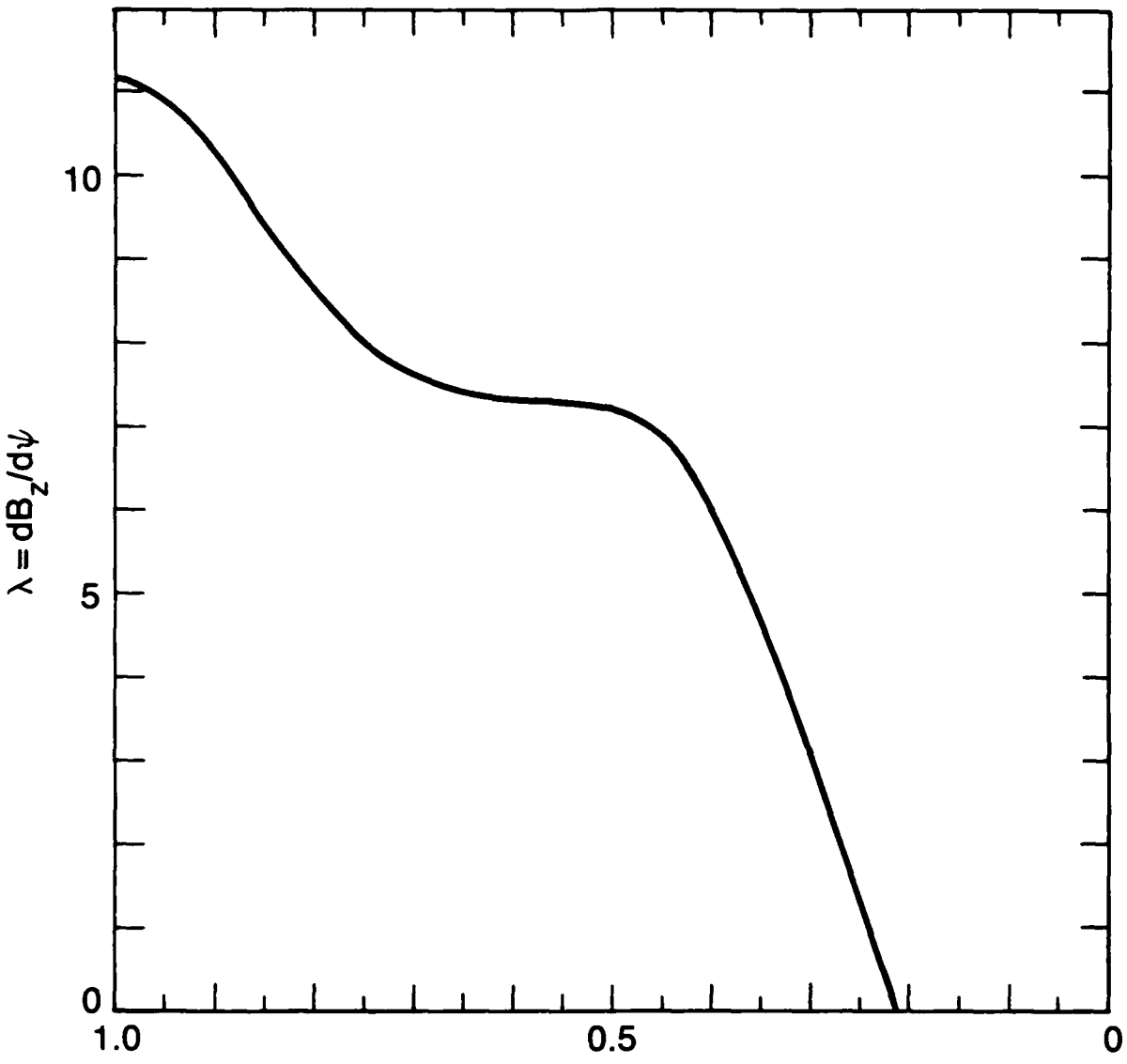

Fig. 6 (Continued) — Equilibrium with parameters as in Fig. 5 except $d_{max} = 0.61$.

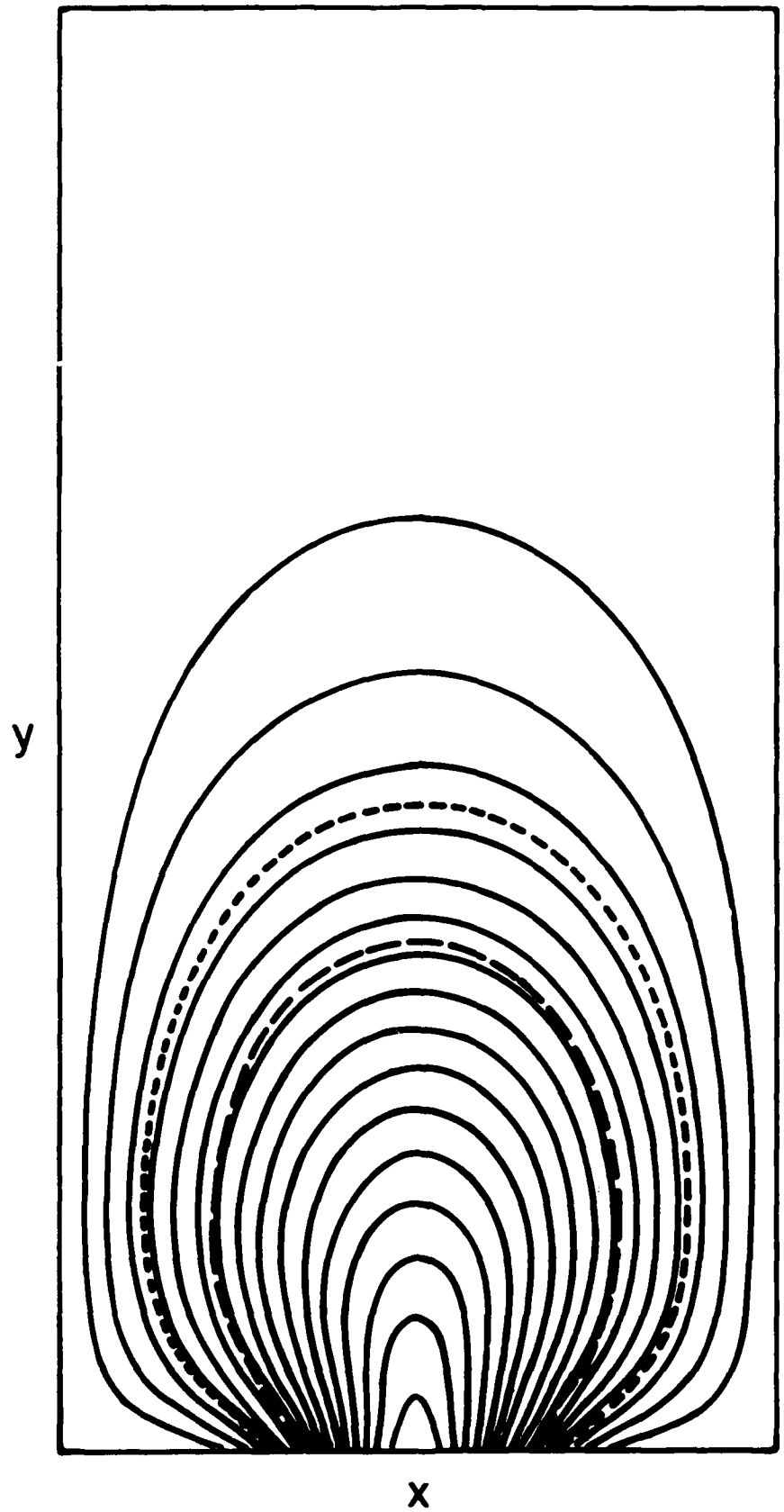

Fig. 7 — Equilibrium with parameters as in Fig. 5 except $d_{max} = 1.35$.

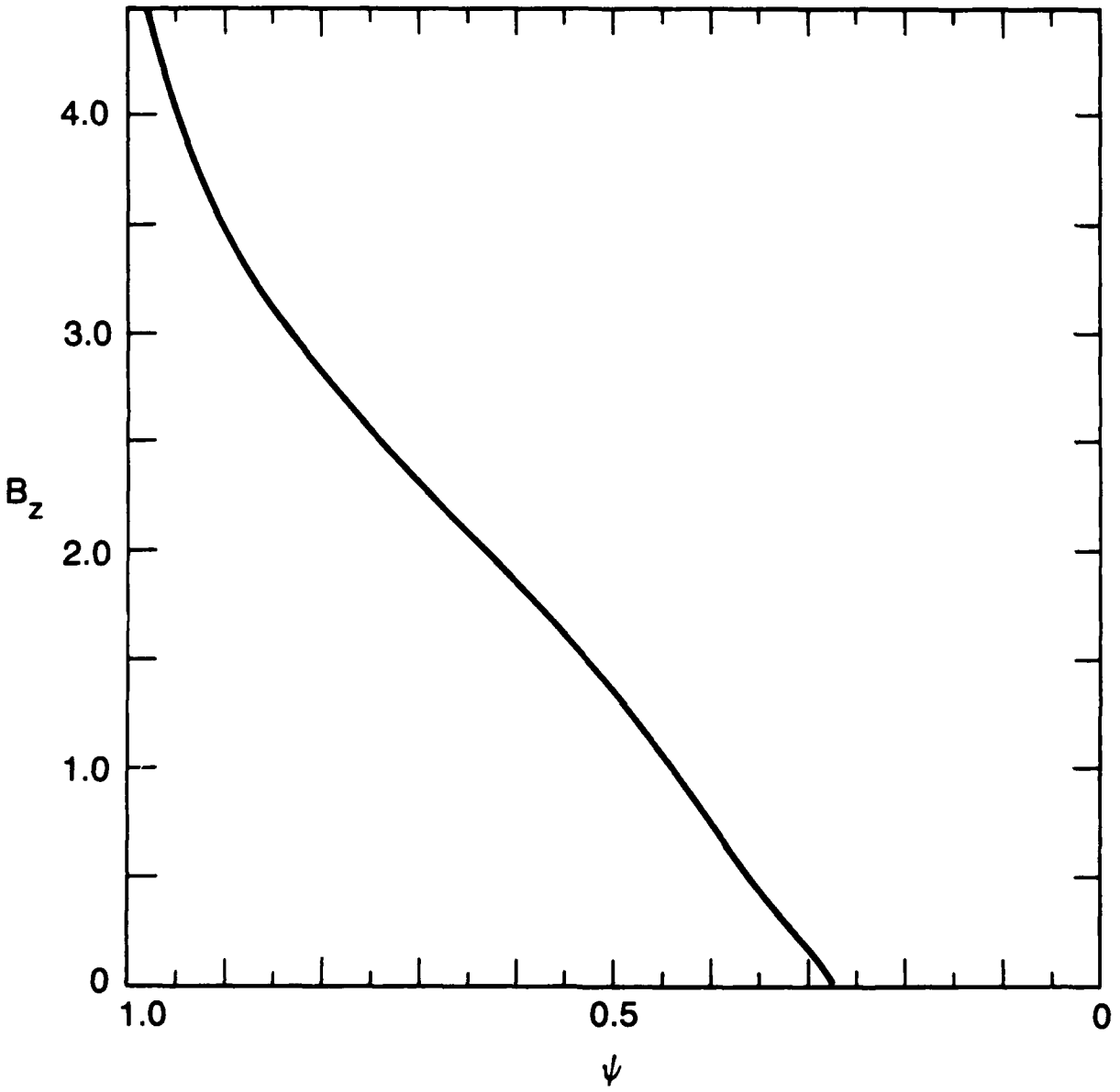

Fig. 7 (Continued) — Equilibrium with parameters as in Fig. 5 except d_{max} = 1.35.

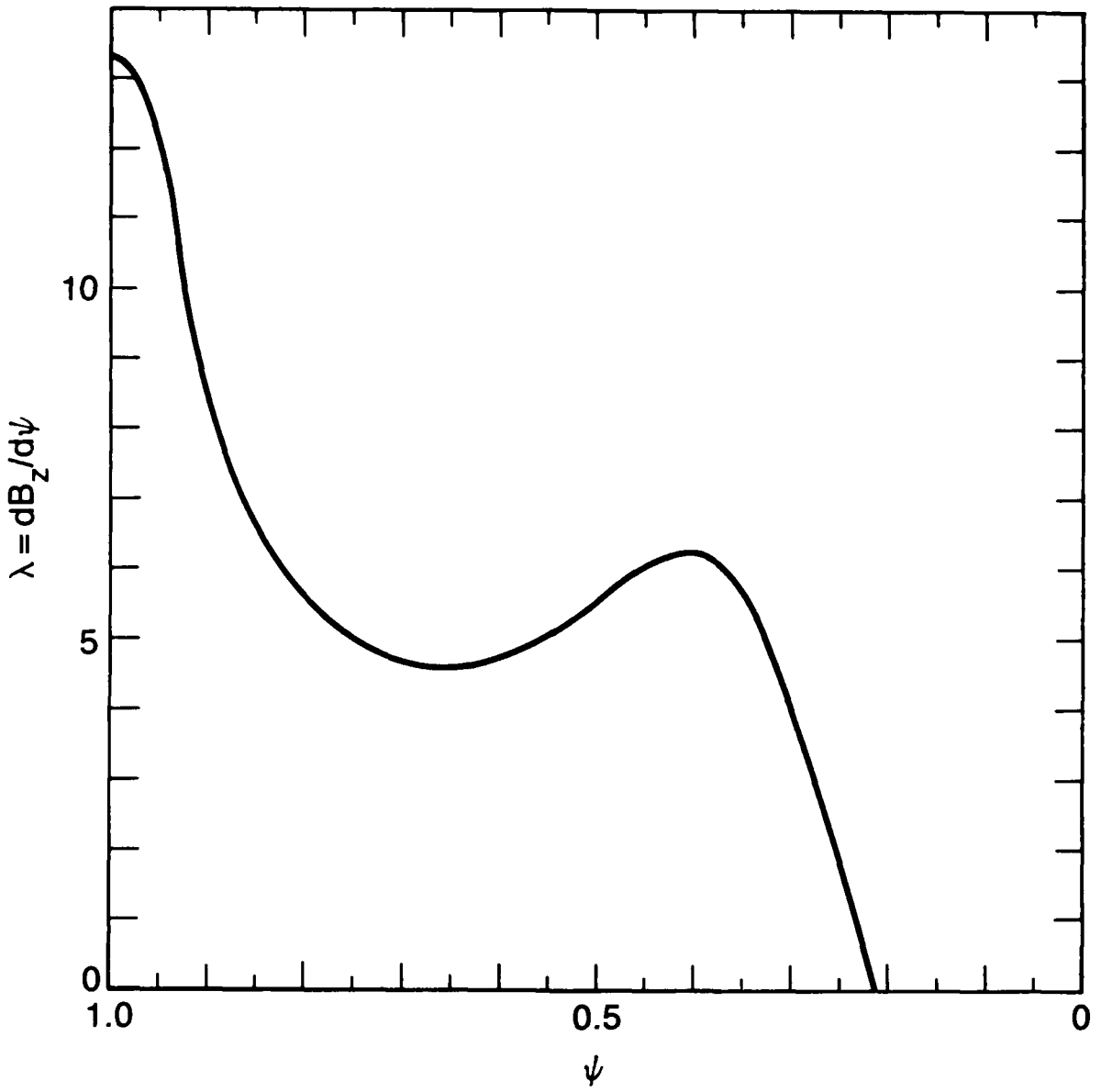

Fig. 7 (Continued) — Equilibrium with parameters as in Fig. 5 except $d_{max} = 1.35$.

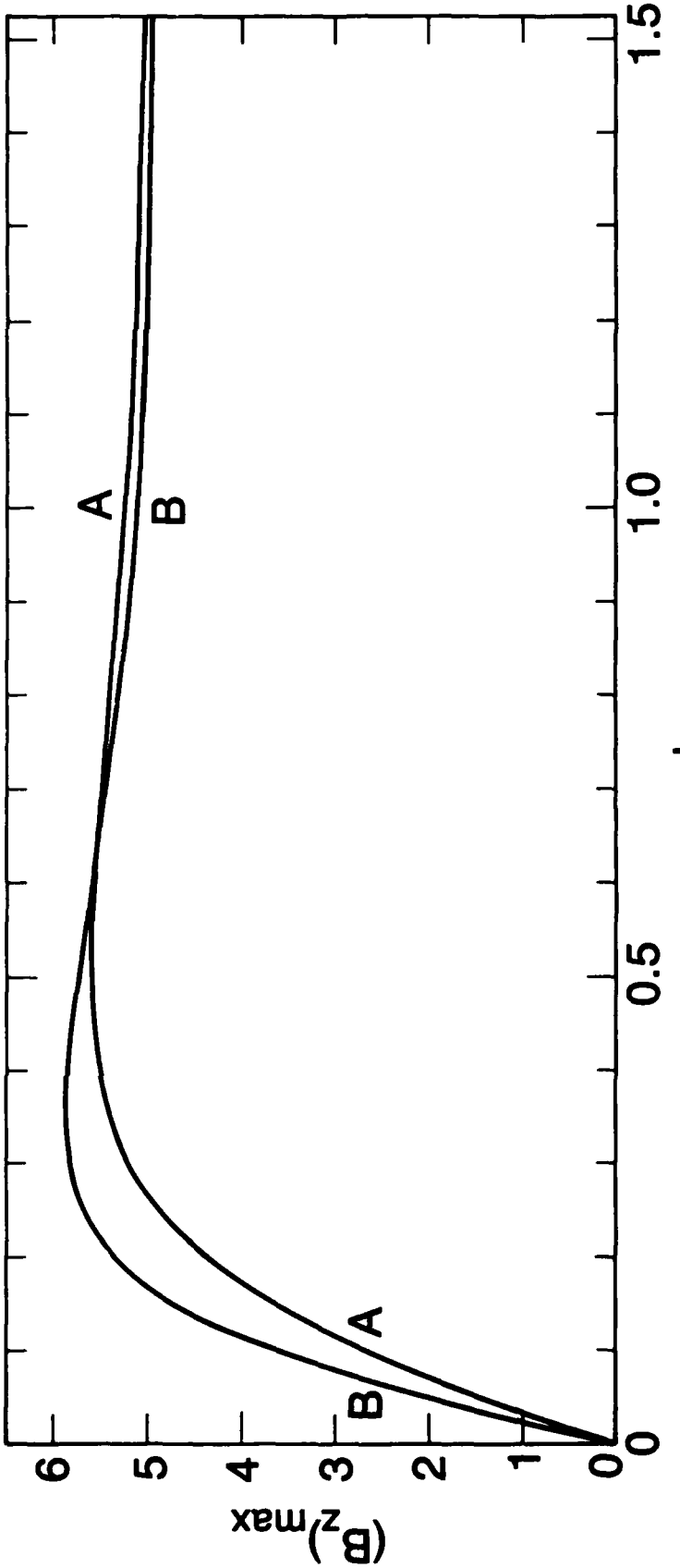

Fig. 8 — $(B_z)_{max}$ versus d_{max} for two series of equilibria. Series B has parameters as in Figs. 5 — 7. Series A has the same parameters, except $\psi_v = 9 \times 10^{-3}$ ($x_v = 0.17$) and W = 0.45.

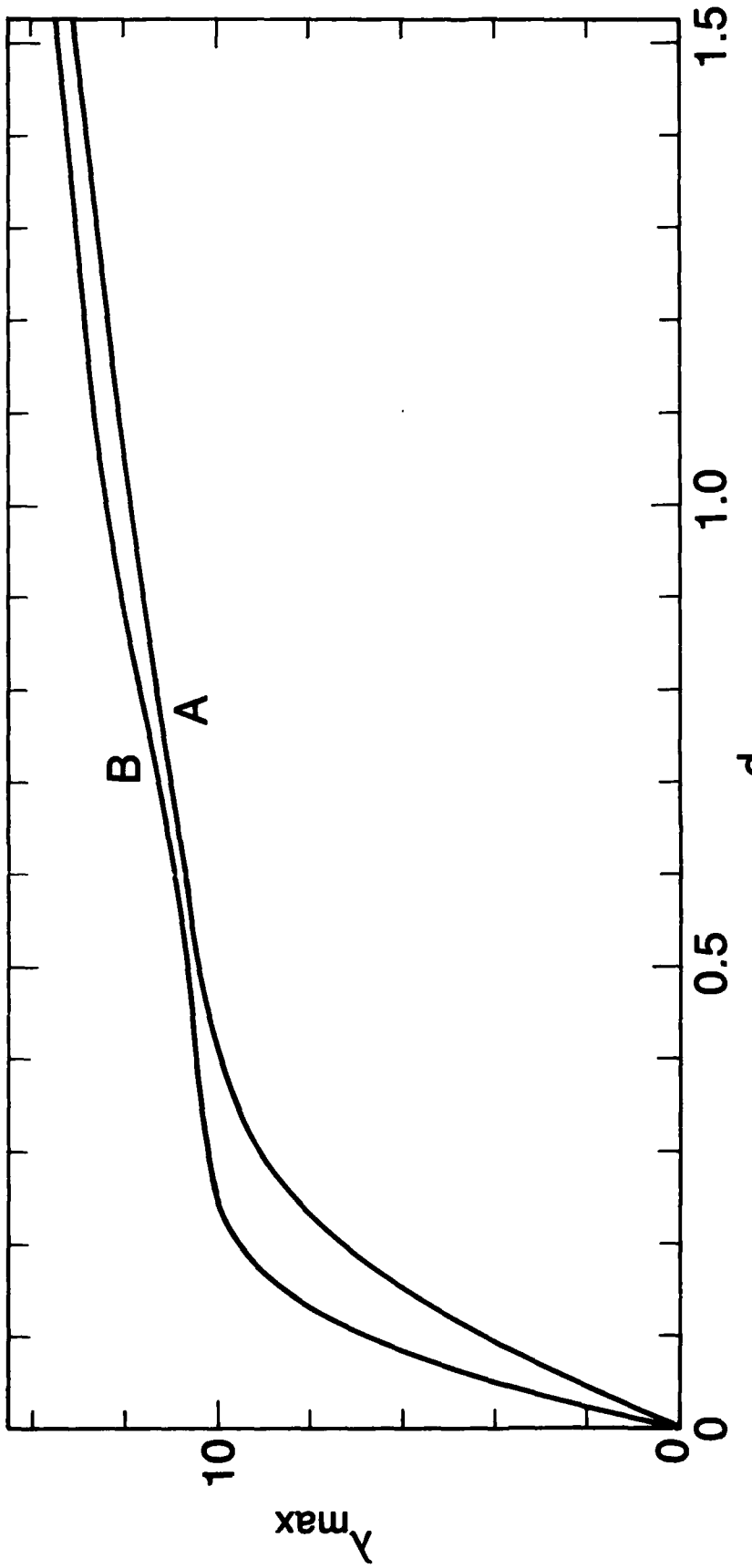

Fig. 9 — The maximum of $\lambda(\psi)$, λ_{max} versus d_{max} for the equilibria of Fig. 8.

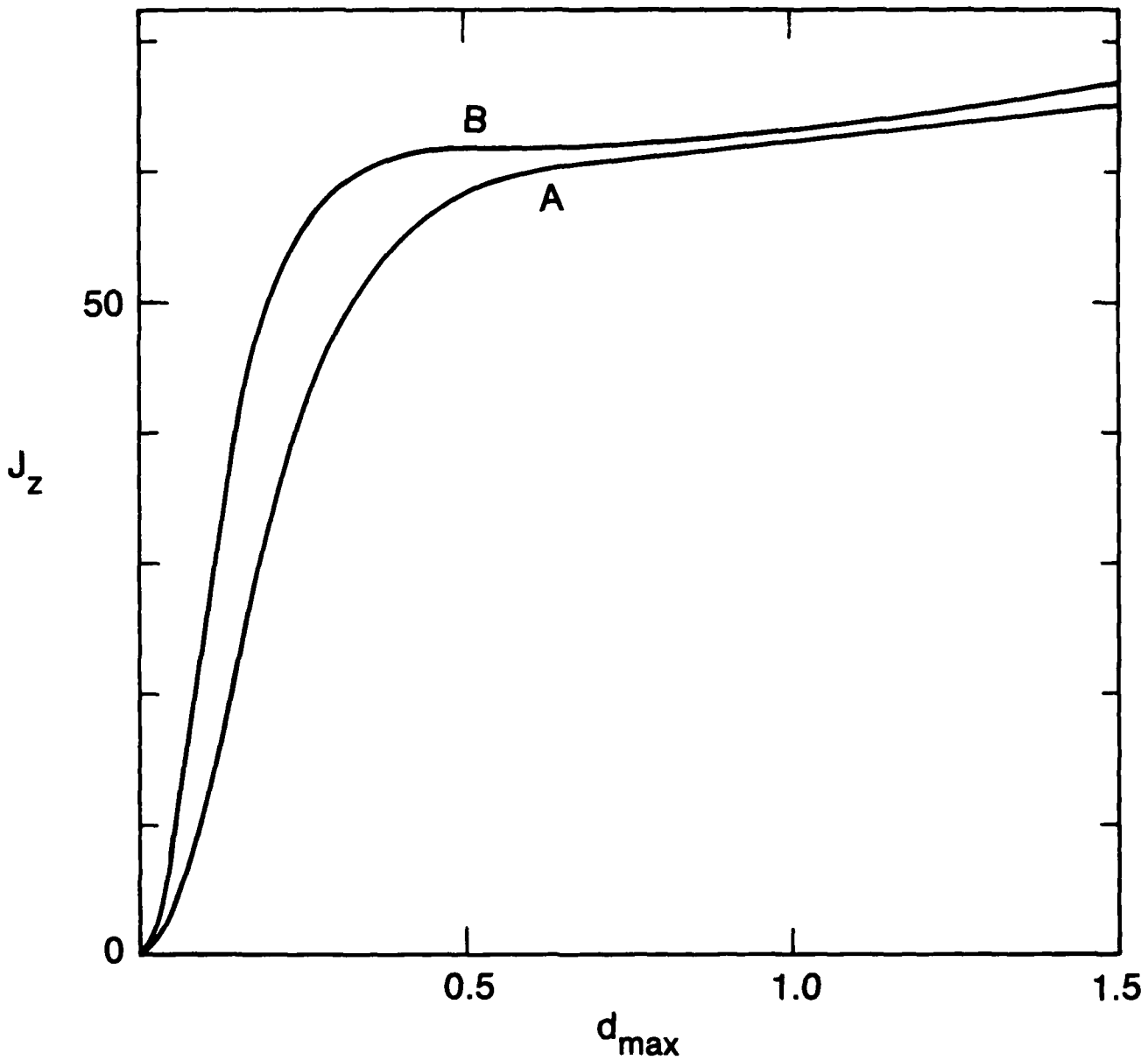

Fig. 10 — Maximum current density j_zl versus d_{max} for the equilibria of Fig. 8.

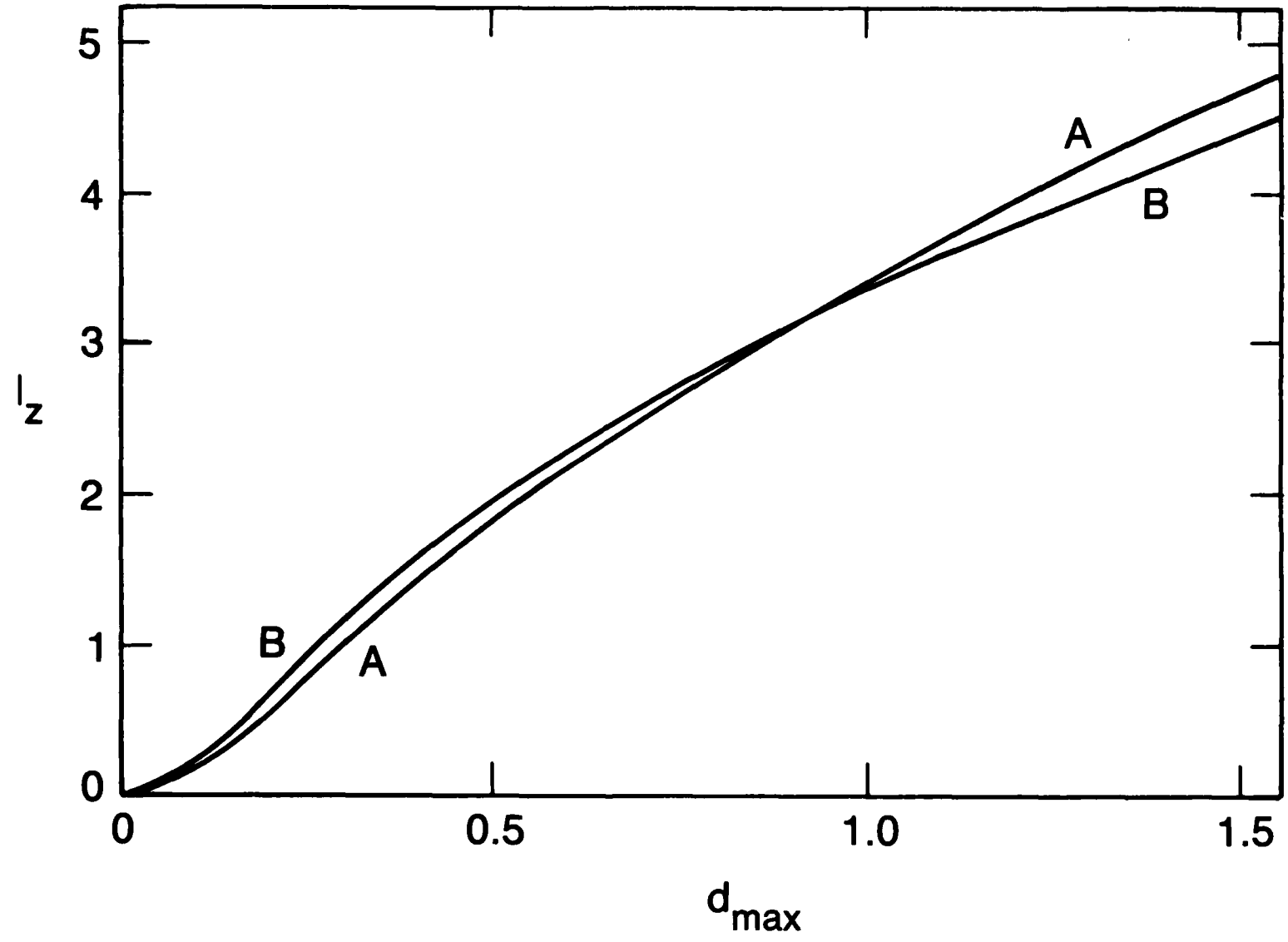

Fig. 11 — Total current I_z versus d_{max} for the equilibria of Fig. 8.

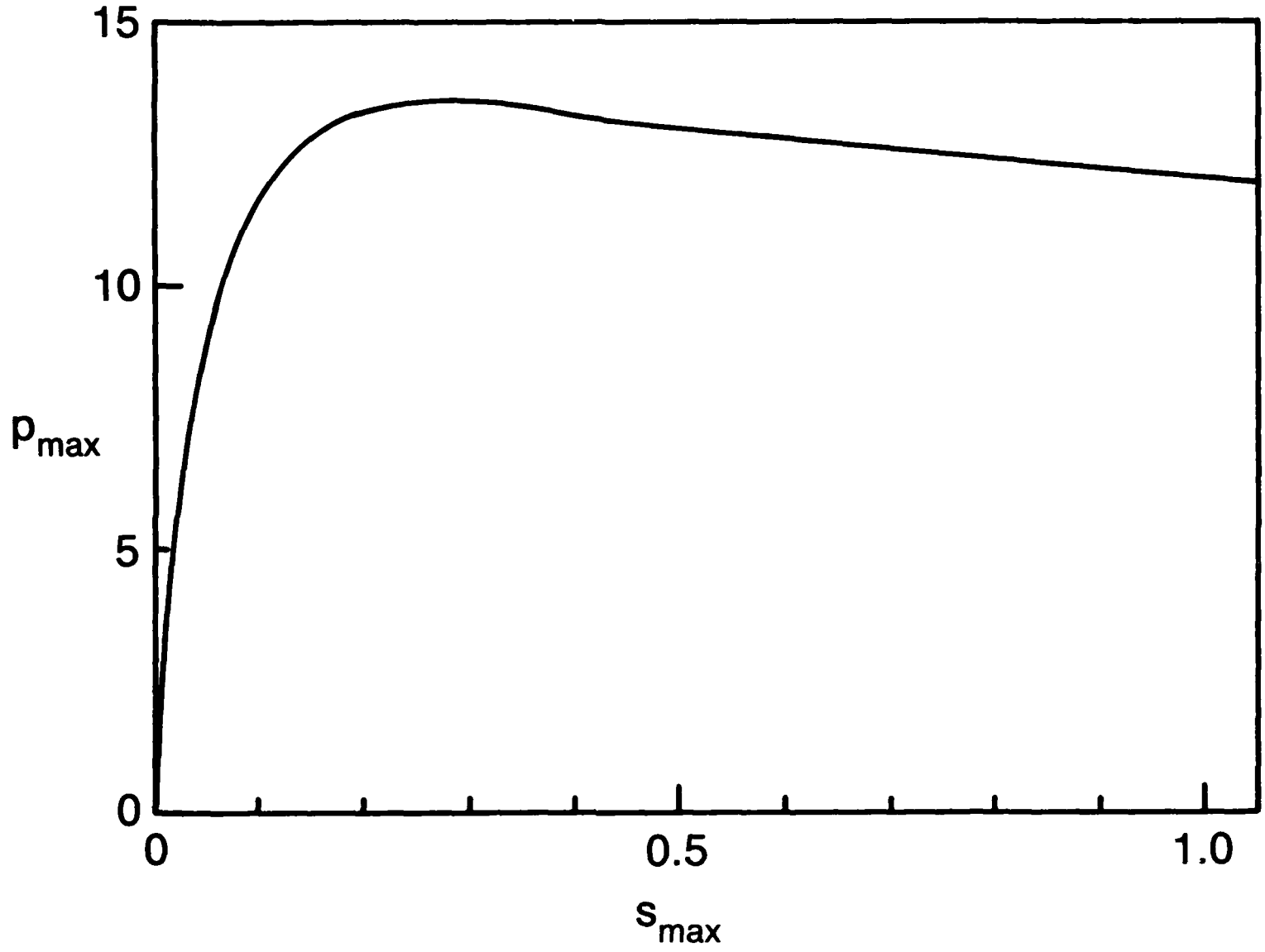

Fig. 12 — Sequence of equilibria with respect to specification of entropy. (a) Maximum pressure p_{max} versus maximum entropy s_{max} for a class of finite β equilibria with $d_{max} = 0$. The form of $s(\psi)$ is given by $[d(\psi)]^{1/2}$, where $d(\psi)$ is the form factor in Eq. (21). The other parameters are those of Figs. 5 — 7 and series B of Fig. 8. (b) Total current I_z and maximum current density j_z versus s_{max}.

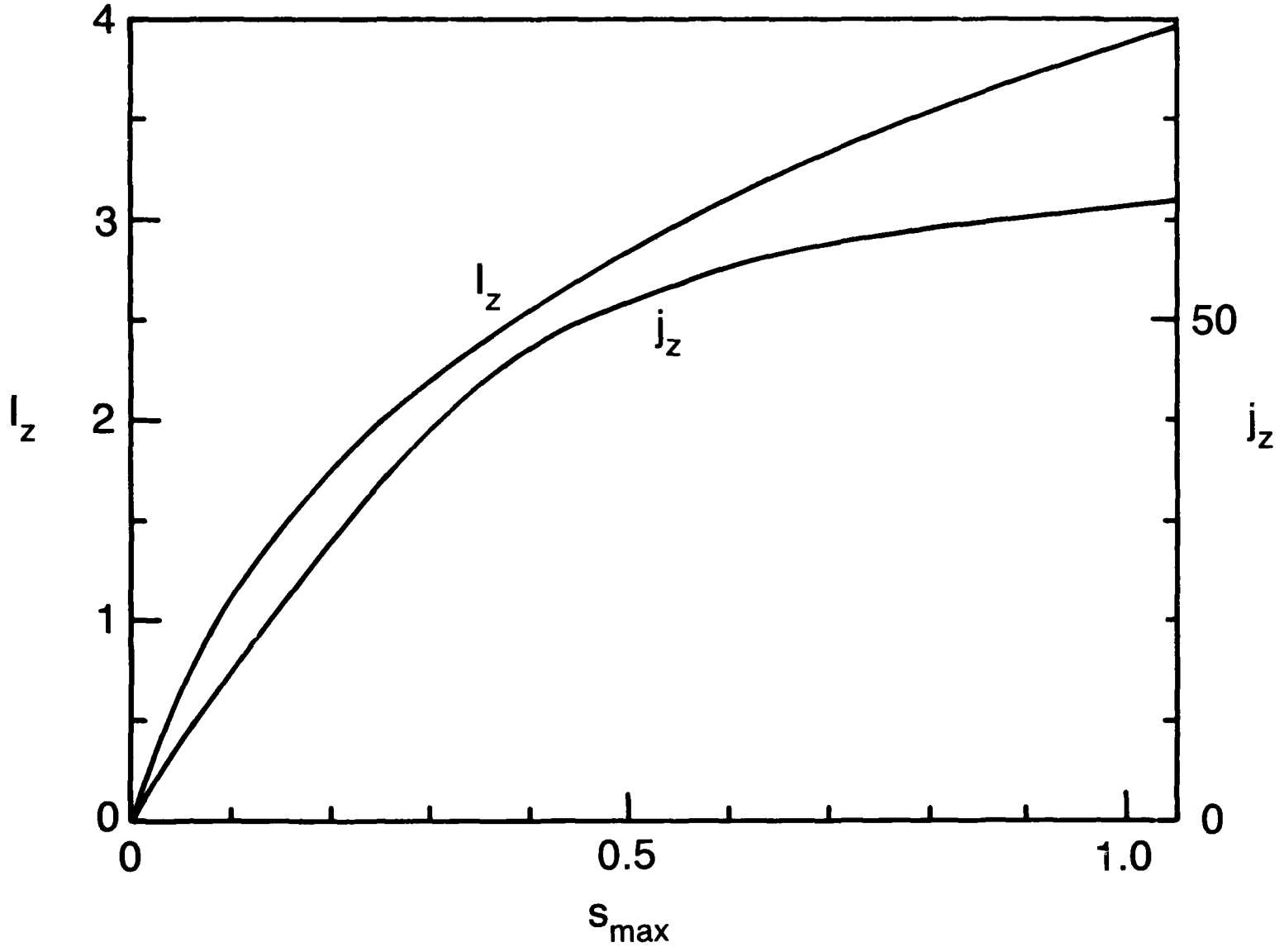

Fig. 12 (Continued) — Sequence of equilibria with respect to specification of entropy. (a) Maximum pressure p_{max} versus maximum entropy s_{max} for a class of finite β equilibria with $d_{max} = 0$. The form of $s(\psi)$ is given by $[d(\psi)]^{1/2}$, where $d(\psi)$ is the form factor in Eq. (21). The other parameters are those of Figs. 5 — 7 and series B of Fig. 8. (b) Total current I_z and maximum current density j_z versus s_{max}.

DISTRIBUTION LIST
(Unclassified Only)

DISTRIBUTE ONE COPY EACH TO THE FOLLOWING PEOPLE (UNLESS OTHERWISE NOTED)

DIRECTOR
NAVAL RESEARCH LABORATORY
WASHINGTON, DC 20375-5000
CODE 4700 (26 CYS)
CODE 4701
CODE 4780 (50 CYS)
CODE 4750 (P. RODRIGUEZ)
CODE 4100
CODE 4172 (N.R. SHEELEY)
CODE 4173
CODE 4160
CODE 4175A
CODE 4175C
CODE 4175M
CODE 4175 (JK)
CODE 4170
CODE 4400
CODE 4440 (R. DAHLBURG)
CODE 4440 (M. PICONE)
CODE 4440 (E. DEVORE)

OFFICE OF NAVAL RESEARCH
WASHINGTON, DC 22203
C. ROBERSON

COMMANDING OFFICER
OFFICE OF NAVAL RESEARCH
WESTERN REGIONAL OFFICE
1030 EAST GREEN STREET
PASADENA, CA 91106
R. BRANDT

NASA HEADQUARTERS
CODE EE
WASHINGTON, DC 20546
S. SHAWHAN
D. BUTLER
T. EASTMAN

NASA/GODDARD SPACE FLIGHT CENTER
GREENBELT, MD 20771
M. GOLDSTEIN, CODE 692
T. NORTHROP, CODE 665
T. BIRMINGHAM, CODE 695.1
SHING F. FUNG, CODE 696
D.S. SPICER, CODE 682
J. DAVILA, CODE 682
L. BURLAGA, CODE 692
A.I. POLAND, CODE 682

AEROSPACE CORPORATION
A6/2451, P.O. BOX 92957
LOS ANGELES, CA 90009
A. NEWMAN
D. GORNEY
M. SCHULZ
J. FENNEL

BELL LABORATORIES
MURRAY HILL, NJ 07974
A. HASEGAWA
L. LANZEROTTI

LAWRENCE LIVERMORE LABORATORY
UNIVERSITY OF CALIFORNIA
LIVERMORE, CA 94551
LIBRARY
J. DEGROOT
B. LANGDON
R. BRIGGS
D. PEARLSTEIN

LOS ALAMOS NATIONAL LABORATORY
P.O. BOX 1663
LOS ALAMOS, NM 87545
S.P. GARY
J. BIRN
D. FORSLUND
J. KINDEL
D. WINSKE
J.T. GOSLING

LOCKHEED RESEARCH LABORATORY
3251 HANOVER STREET
PALO ALTO, CA 94304
M. WALT
L.W. ACTON

NATIONAL SCIENCE FOUNDATION
ATMOSPHERIC RESEARCH SECTION
WASHINGTON, DC 20550
D. PEACOCK

UNIVERSITY OF ALASKA
GEOPHYSICAL INSTITUTE
FAIRBANKS, AK 99701
LIBRARY
S. AKASOFU
J. KAN
L. LEE

UNIVERSITY OF ARIZONA
DEPT. OF PLANETARY SCIENCES
TUCSON, AZ 85721
J.R. JOKIPII

UNIVERSITY OF CALIFORNIA, S.D.
LAJOLLA, CA 92037
(PHYSICS DEPARTMENT):
T. O'NEIL
H.S. HUDSON, MC C-011
B.V. JACKSON
LIBRARY

UNIVERSITY OF CALIFORNIA
SPACE SCIENCE LABORATORY
BERKELEY, CA 94720
M. TEMERIN
F. MOZER

UNIVERSITY OF CALIFORNIA
IRVINE, CA 92664
(PHYSICS DEPARTMENT):
LIBRARY
G. BENFORD

UNIVERSITY OF CALIFORNIA
LOS ANGELES, CA 90024
(PHYSICS DEPARTMENT):
J.M. DAWSON
W. GEKELMAN
R. STENZEL
F. CHEN
LIBRARY
R. WALKER
(INSTITUTE OF GEOHPYSICS
AND PLANETARY PHYSICS):
LIBRARY
C. KENNEL
F. CORONITI

UNIVERSITY OF CALIFORNIA
DEPT. OF PHYSICS
IRVINE, CA 92717
G. VAN HOVEN
L. SPARKS

UNIVERSITY OF CHICAGO
ENRICO FERMI INSTITUTE
CHICAGO, IL 60637
E.N. PARKER
R. ROSNER
I. LERCHE
LIBRARY

UNIVERSITY OF COLORADO
DEPT. OF ASTROPHYSICAL,
PLANETARY AND ATMOSPHERIC
SCIENCES
BOULDER, CO 80309
M. GOLDMAN
E. ZWEIBEL
T. CHLUEH
LIBRARY

CORNELL UNIVERSITY
SCHOOL OF APPLIED AND
ENGINEERING PHYSICS
COLLEGE OF ENGINEERING
ITHACA, NY 14853
LIBRARY
R. SUDAN
B. KUSSE
H. FLEISCHMANN
R. LOVELACE
(SCHOOL OF ELECTRICAL
ENGINEERING):
N. OTANI

HARVARD UNIVERSITY
CENTER FOR ASTROPHYSICS
60 GARDEN STREET
CAMBRIDGE, MA 02138
G.B. FIELD
K. TSINGANOS
G.S. VAIANA
Q.L. WITHBROE

UNIVERSITY OF IOWA
IOWA CITY, IA 52240
C.K. GOERTZ
L.A. FRANK
K. NISHIKAWA
N. D'ANGELO

UNIVERSITY OF MARYLAND
PHYSICS DEPARTMENT
COLLEGE PARK, MD 20742
K. PAPADOPOULOS
C. WU
P. CARGILL
J. DRAKE
A.B. HASSAM

M.I.T.
CAMBRIDGE, MA 02139
LIBRARY
(PHYSICS DEPARTMENT):
B. COPPI
T. CHANG
R. DAVIDSON
(R.L.E): LIBRARY
(SPACE SCIENCE):
READING ROOM

UNIVERSITY OF NEW HAMPSHIRE
DEPARTMENT OF PHYSICS
DURHAM, NH 03824
R.L. KAUFMAN
J. HOLLWEG

PRINCETON UNIVERSITY
PRINCETON, NJ 08540
PHYSICS LIBRARY
(PLASMA PHYSICS LAB.):
LIBRARY
F. PERKINS
T.K. CHU
H. OKUDA
R. KULSRUD
H. FURTH

STANFORD UNIVERSITY
CENTER FOR SPACE SCIENCE
AND ASTROPHYSICS
STANFORD, CA 94305
P.A. STURROCK
J. KLIMCHUK
T. BAI

STEVENS INSTITUTE OF TECHNOLOGY
HOBOKEN, NJ 07030
B. ROSEN
G. SCHMIDT
M. SEIDL

UNIVERSITY OF TEXAS
AUSTIN, TX 78712
W. HORTON

THAYER SCHOOL OF ENGINEERING
DARTMOUTH COLLEGE
HANOVER, NH 03755
BENGT U.O. SONNERUP
M. HUDSON

UTAH STATE UNIVERSITY
DEPT. OF PHYSICS
LOGAN, UT 84322
ROBERT W. SCHUNK

UNIVERSITY OF THESSALONIKI
DEPARTMENT OF PHYSICS
GR-54006 THESSALONIKI,
GREECE
L. VLAHOS

NASA MARSHALL SPACE
FLIGHT CENTER
HUNTSVILLE, AL 35812
C.H. AN, ES-52
J. PORTER, ES-52
J. FONTENLA, ES-52

UNIVERSITY OF ALABAMA, HUNTSVILLE
DEPARTMENT OF PHYSICS
HUNTSVILLE, AL 35899
A.G. EMSLIE
(MECHANICAL ENGINEERING):
S.T. WU

MIDDLEBURY COLLEGE
DEPT. OF PHYSICS
MIDDLEBURY, VT 05733
R. WOLFSON

UNIVERSITY OF HAWAII
INSTITUTE FOR ASTRONOMY
2680 WOODLAWN DRIVE
HONOLULU, HI 96822
G. FISHER
R. CANFIELD
A.N. McCLYMONT

HIGH ALTITUDE OBSERVATORY/NCAR
P.O. BOX 3000
BOULDER, CO 80307
A. CHOUDHURI
E. HILDNER
B.C. LOW
A. HUNDHAUSEN
T.E. HOLZER
R.M. MacQUEEN
V. PIZZO
D.G. SIME

INSTITUTE OF THEORETICAL PHYSICS
RUHR-UNIVERSITAT BOCHUM
4630 BOCHUM, WEST GERMANY
K. SCHINDLER

THE UNIVERSITY OF ST. ANDREWS
APPLIED MATHEMATICS DEPT.
ST. ANDREWS, SCOTLAND
E.R. PRIEST

UNIVERSITY OF TEXAS, AUSTIN
DEPT. OF PHYSICS
AUSTIN, TX 78712
T. TAJIMA
R.S. STEINOLFSON

BERKELEY RESEARCH ASSOCIATES
290 GREEN ROCK DRIVE
BOULDER, CO 80302
D.F. SMITH

APPLIED PHYSICS LABORATORY
THE JOHNS HOPKINS UNIVERSITY
LAUREL, MD 20707
A.T.Y. LUI
D.G. MITCHELL
D.A. BATCHELOR

SCIENCE APPLICATIONS INTERNATIONAL
CORPORATION
10260 CAMPUS POINT DRIVE
SAN DIEGO, CA 92121
D.C. BARNES
D.D. SCHNACK
Z. MIKIC

YALE UNIVERSITY
CENTER FOR SOLAR AND
SPACE RESEARCH
P.O. BOX 6666
NEW HAVEN, CT 06511
I.B. BERNSTEIN
P.A. FOX
S. SOFIA
P. DEMARQUE

COURANT INSTITUTE OF
MATHEMATICAL SCIENCES
NEW YORK UNIVERSITY
NEW YORK, NY 10012
H.R. STRAUSS
E. HAMEIRI
W. LAWSON

MAX-PLANCK INSTITUT FUR
PHYSICS UND ASTROPHYSICS
D-8046
GARCHING, WEST GERMANY
U. ANZER